Spring 2024

Numerical Analysis of a Multi-Stage Elastohydrodynamic Seal for Aircraft Engines

Md Wasif Hasan

NUMERICAL ANALYSIS OF A MULTI-STAGE ELASTOHYDRODYNAMIC SEAL FOR AIRCRAFT ENGINES

by

MD WASIF HASAN

(Under the Direction of Sevki Cesmeci)

ABSTRACT

At present, both governmental and private aviation enterprises are trying to develop aircraft that are swifter, more lightweight, and more cost-effective in order to maintain competitiveness on both the domestic and global stage. Continuous innovation and sustainability efforts are necessary to achieve advancements in aviation systems, such as fans, compressors, combustors, and turbines, as well as sub-systems, like engine seals. Advanced engine seals exhibit considerable potential in enhancing the engine's pressure ratio and cycle temperatures, leading to reduced engine weight, increased thrust, and improved fuel economy. In this study, a novel multistage seal idea has been proposed for the supercritical carbon dioxide (sCO_2) heat recovery unit for aircraft engines that utilizes the established Elastohydrodynamic (EHD) lubrication theory. This study utilized a physics-based computer simulation modeling technique. Because of the complex and non-linear interactions between the seal and the fluid domain in Fluid-Solid-Interactions (FSI), a design approach that combines Finite Element Analysis (FEA) and Computational Fluid Dynamics (CFD) was used. Utilizing the latest advancements in commercially accessible software, the COMSOL Multiphysics program was utilized to conduct fully linked FSI simulations. The modeling technique was comprehensively explained, and the findings were fully examined. The leakage was found to be 0.016 kg/s at 19 MPa. The suggested seal system has the potential to serve as a substitute for the current sealing technologies available in the market.

INDEX WORDS: Seal, Aircraft, Elastohydrodynamic, Numerical, Fluid-solid interaction simulation, CFD, Solid mechanics, Gas turbine, Turbomachinery.

NUMERICAL ANALYSIS OF A MULTI-STAGE ELASTOHYDRODYNAMIC SEAL FOR AIRCRAFT ENGINES

by

MD WASIF HASAN

B.S., Khulna Engineering University & Technology, Bangladesh, 2018

A Dissertation (or Thesis) Submitted to the Graduate Faculty of Georgia Southern University

in Partial Fulfillment of the Requirements for the Degree

MASTER OF SCIENCE

STATESBORO, GEORGIA

NUMERICAL ANALYSIS OF A MULTI-STAGE ELASTOHYDRODYNAMIC SEAL FOR AIRCRAFT ENGINES

by

MD WASIF HASAN

Major Professor:	Sevki Cesmeci
Committee:	Priya Goeser
	Prakashbhai Bhoi

Electronic Version Approved:

May 2024

DEDICATION

In recognition of their support throughout this endeavor, I dedicate this work to my family and friends.

ACKNOWLEDGMENTS

I would like to express my gratitude to Dr. Sevki Cesmeci for his unwavering support throughout my time as a graduate student at Georgia Southern University. I would like to express my gratitude to my lab mates, Mohammad Fuad Hassan, Mohammad Towhidul Islam, and Ali Akbor Topu, for their invaluable support and aid. I express my gratitude to Dr. Priya Goeser and Dr. Prakashbhai Bhoi, who served as members of my committee, for their valuable time and advice.

TABLE OF CONTENTS

Page

LIST OF TABLES

Page

LIST OF FIGURES

Page

CHAPTER 1

INTRODUCTION

Aircraft engines are heat engines that convert the energy generated by fuel combustion into mechanical energy. As a result, the propulsion system of the airplane engine employs mechanical energy to produce thrust. Depending on the kind and use of the jet engine, the thrust varies. However, a plane's engine efficiency is determined by how much fuel it uses to produce thrust. Specifically, the ratio of fuel mass flow rate to the amount of thrust generated is known as thrust-specific fuel consumption. The thrust-to-weight ratio is another crucial engine design factor in addition to specific fuel consumption. The better the engine's weight-to-thrust ratio, the less fuel is required to lift, carry the engine's weight, or accelerate it. Bypass air and hot combustion product gas from the main engine compose the mixed exhaust of turbofans. The ratio of air entering a turbofan's core engine to air leaving it is known as the bypass ratio. High bypass ratio engines are recommended for commercial airplanes due to their improved fuel efficiency and reduced noise levels.

Over the past years, a lot of research has been conducted to improve fuel economy. Improved component performance and reduced engine deterioration can improve fuel consumption by up to 5 percent (Sens 1979). Increasing the overall pressure ratio and reducing cooling air requirements can enhance fuel efficiency (Heidmann 2013). (Millhouse 1998) introduces automated techniques and optimization processes to minimize fuel consumption and obtain optimal engine solutions.

Along with fuel efficiency, another important design factor is to reduce fuel emissions to the environment. There have been several recent developments in addressing

the pollution problem, such as green fuel, sustainable fuel solutions, and the development of hybrid and electric airplanes. According to recent studies, newer models of the Boeing 737 and Airbus A320 increased passenger capacity while using 23% less fuel than prior models (Chopra 2019)

According to a recent estimate, the global total fleet will reach 37978 by 2028, up from 26,307 in 2018. ("GLOBAL FLEET & MRO MARKET FORECAST COMMENTARY" 2018) The rising demand in the aviation sector raises concerns about the use of fossil fuels, their emissions, and costs. Prior to the pandemic, US airlines used $36 billion on fuel, but the figure has dropped by 25.3% to $27 billion in 2021. (Bureau of Transportation Statistics 2022). In 2022, US airlines spent $56 billion on fuel, a 64% increase over 2019 (Kemp 2023). Figure 1 shows the consumption of fuel by US Airlines over the year.

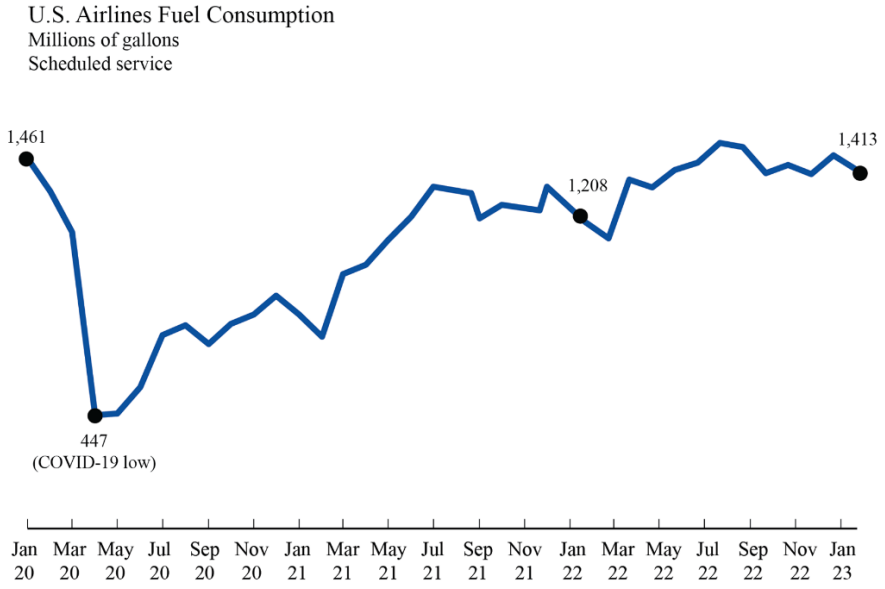

Figure 1 U.S. Airlines fuel consumption from January 2020 to January 2023. (Bureau of Transportation Statistics 2023)

Aside from economic considerations, the aviation sector was responsible for 2.4 percent of worldwide carbon emissions in 2018, which was 1.9% in 2016(Ritchie 2020). Carbon dioxide (CO_2) is the main contributor to global warming. In 2023, the U.S. was responsible for 4.38 billion metric tons of CO_2 production (Energy Information Administration 2024). The number of emissions will triple by 2050 due to the predicted increase in the aviation sector (Overton 2022). The U.S. Department of Energy and the International Civil Aviation Organization (ICAO) have been working relentlessly to replace fossil fuels with sustainable fuels to emit less carbon from combustion (International Civil Aviation Organization 2016).

1.1 Problem Statement

In order to improve engine efficiency while keeping its size and weight constant, pressure ratio is one of the aspects that must be considered. It also increases the temperature at the turbine inlet and outlet. One way to improve the overall efficiency of the system is by using waste heat (Vesely et al. 2021) in a power cycle, such as a steam Rankine cycle, organic Rankine cycle (ORC), or a supercritical CO2 Brayton cycle (Carcasci and Winchler 2016). For reducing carbon emissions, utilization of waste heat recovery unit in aircraft engines is one of the potential solutions (Khadse et al. 2018; Pasini et al. 2002). However, leakage must be kept to a minimum to raise the pressure ratio, oil leakage, and emission. The engine's sealing system must be enhanced to prevent unintended leakage, raising the pressure ratio. However, the current sealing system was unable to stop this type of leakage and maintain sustainability in high-temperature conditions.

One of the most used and popular seals in aviation engines is the labyrinth seal. However, the space between the shaft and the teeth and the leakage rate are related (Kim et

al. 2019). Additionally, the effectiveness of the labyrinth seal is significantly influenced by shaft speed and input and outlet temperatures (Wu and San Andrés 2019). Due to usage over time, the brush seal deteriorated, which increased the leakage rate (Ferguson 1988). Additionally, brush seals are used to function at a relatively low temperature (B. M. Steinetz, Hendricks, and Munson 1998). In contrast, a face seal may prevent leaks but only at low pressure, which is very unlikely in a jet engine (B. M. Steinetz, Hendricks, and Munson 1998).

To address these problems, a non-contact, high-temperature, and high-pressure compatible elastohydrodynamic seal based on proven elastohydrodynamic lubrication theory was proposed. (Cesmeci et al. 2021). In this study, numerical analysis will be carried out for multistage elastohydrodynamic seals for waste heat recovery unit in aircraft engines. The simulations will be performed using the COMSOL Multiphysics program, and the Hi-Mach Number Flow and Solid Mechanics modules will be coupled and used to solve the fluid and solid domains, respectively.

1.2 Hypothesis

Recent studies illustrate the importance of the development of sealing technology in terms of leakage and maintenance. If the proposed concept, based on proven elastohydrodynamic lubrication theory, can be applied in the design methodology of modern aircraft engine seals, the leakage rate will improve significantly compared to the existing sealing solution. In addition to that, the proposed seal concept based on elastohydrodynamic theory will increase flexibility in maintenance and scalability.

The hypothesis will be proven when the proposed seal concept's experimental result follows the numerical result which will be carried out by fluid-solid interaction simulation in COMSOL Multiphysics simulation software.

CHAPTER 2

LITERATURE REVIEW

The aviation sector has been undergoing constant development since its beginning. From an aesthetic to a technological standpoint, every small modification has been seen as a significant advancement in the aviation business. However, the most complicated component of an airplane is its engine. In the beginning, a reciprocating engine was utilized as an airplane engine. Gas turbines replaced the reciprocating engine as the most efficient option for jet propulsion after 1960. Gas turbines are now available in the form of various jet engines to meet a variety of needs.

2.1 Jet Engine

Gas turbines, regardless of their design or size, operate on a relatively basic concept. It is based on the Brayton cycle, in which air is continually fed into the engine. A Boeing 747 engine typically has 40,000 pieces, and part numbers range from 25,000 to 50,000 for jet engines. The number of engine components, however, is independent of whether the engine body is large or narrow. Newer engines, on the other hand, are said to contain fewer components than older engines due to technical advancements in the manufacturing process and characteristic advancement in material properties. The jet engine has six major components. Figure 2 shows the schematics of a jet engine.

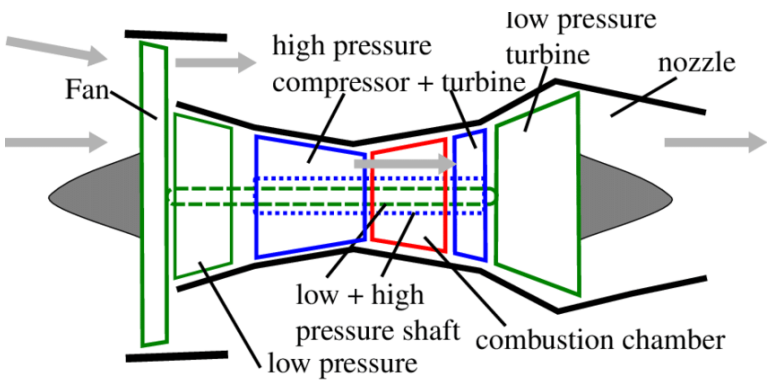

Figure 2 Schematic diagram of turbojet engine (Schriber 2016)

The first main component is the turbofan, which takes air from the surroundings and channels it through two distinct paths. The air is immediately pumped into the core portion in one channel, while the air is bypassed in the other to cool down the other components (Shaw 2021) The turbo-compressor is made up of several rotating blades and stationary vanes that work together to generate a sequence of compression stages. The air is compressed up to 10 to 40 times its intake as it passes through these small openings. The air in the combustion chamber comes into contact with a steady stream of hydrocarbon fuel and burns at a constant pressure. At this constant pressure, the average temperature in the combustion chamber is 980 to 1540 °C. Figure 3 shows the working fluid's operational state. Some of the components in the combustion chamber are constructed of ceramic material due to the high temperature. The hot, expanding, high-energy air afterward enters the turbine section, which contains the same rotating and stationary components as the compressor section. As the turbine is attached to a shaft, the energy from the airflow is used to rotate the compressor and fan. Finally, the nozzle uses the released energy from the turbine to generate thrust. (Baxter and Ehrich 2024)

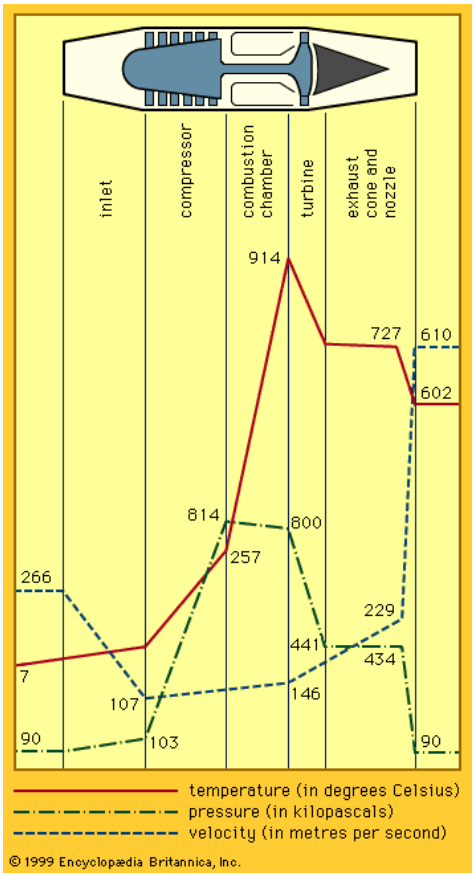

Figure 3 Graph of the operating condition of working fluid (Baxter and Ehrich 2024)

2.2 Engine Classification

The operation of a gas turbine is identical to that of its kind. However, jet engines are classed according to the number of spools, compression ratio, airflow, pressure, and temperature, as well as exhaust gas properties. Turbojet, turbofan, turboprop, and turboshaft are the most popular types of turbine engines used in aircraft. Figure 4 illustrates a comparison of the propulsion efficiency of several jet engines. Regardless of engine type, engines are distinguished by their propulsion characteristics. The flying speed of one kind is directly related to their high jet velocity, but the jet velocity of the other type is inversely proportional to the size of their propellers. (Baxter and Ehrich 2024)

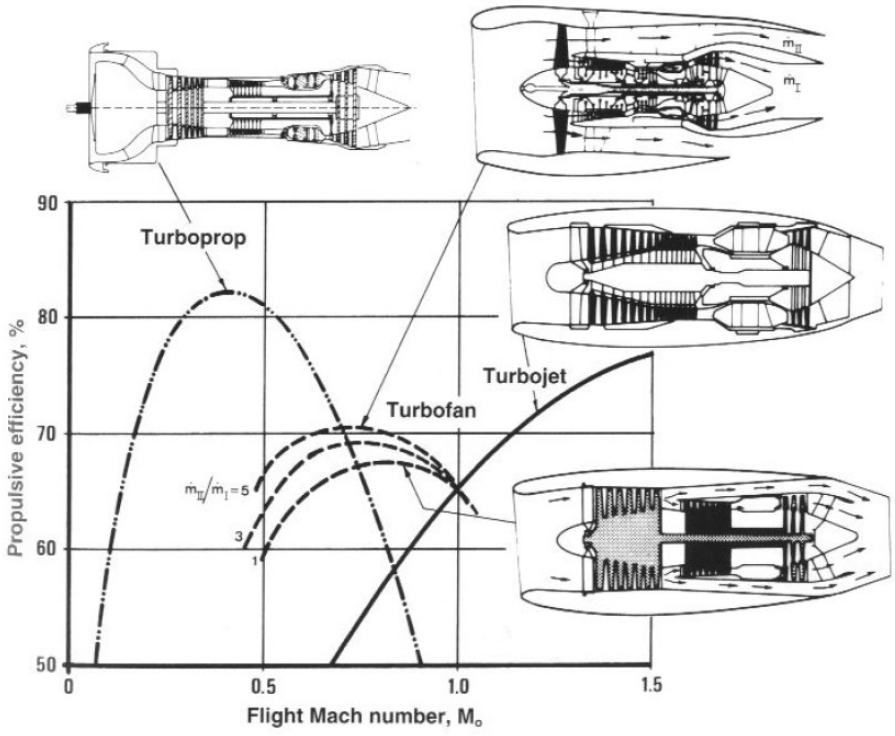

Figure 4 Propulsive efficiency characteristics of turboprop, turbofan, and turbojet engines (Hünecke 1997)

The turbojet engine is a reaction-type engine in which high-energy gas spins the turbine and compressor while gases bounce back and shoot through the exhaust. Meanwhile, the shaft of turboprop engines is attached to a propeller, which is likewise turned by the turbine. When flying at speeds less than 500 miles per hour, turboprop engines outperform turbojet engines in terms of propulsion efficiency. The most common engine is the turbofan engine, which is quieter and produces higher thrust at low speeds. The large fan focuses a part of the air into the core while bypassing the remainder. The bypass is used to enhance thrust without increasing fuel consumption. Another form is the turboshaft, which is frequently used in helicopters. Turboshaft engines are similar to turboprop engines in that

they power the helicopter's rotor rather than the propeller. The rotor speed in this arrangement is independent of the spinning speed of the gas turbine. (Shaw 2021)

2.3 sCO_2 Waste Recovery Unit

Supercritical carbon dioxide (sCO_2) refers to the condition of CO_2 when it is at or beyond its critical point, and there is no separation of liquid and gas phases. Given the critical temperature of 30.98˚C and critical pressure of 7.4 MPa, CO_2 may easily reach a supercritical state. Supercritical carbon dioxide generally has a greater density compared to other working fluids such as steam and water. This allows for significant downsizing of the engine system components. The amount of mechanical labor needed to pressurize the fluid is significantly decreased for sCO_2, resulting in an indirect increase in cycle efficiency and power output (Marchionni, Bianchi, and Tassou 2020). The minimum pressure for the sCO_2 power cycle is 7.4 MPa, in contrast to a steam Rankine cycle which only reaches a few kPa. By making an approximate comparison, the size of the turbomachinery needed for it will be 10 times lower than that necessary for a steam Rankine cycle (Ahn et al. 2015).

There are several factors unique to the aviation industry that make heat recovery more difficult than in the energy sector. These include volume and weight restrictions, severe operating conditions (such as vibration), and dependability standards. All things considered; the waste heat recovery (WHR) system offers a different option for aircraft to enhance their propulsion performance.

Being very compact and lightweight, both the Organic Rankine cycle (ORC) and the sCO_2 Brayton cycle can be used in aircraft engines. The ORC systems use several working fluids (Macchi and Astolfi 2016; de Campos et al. 2020; Bonolo De Campos et al. 2019), which may not be ideal for recovering waste heat in aviation engines. In contrast, sCO_2

systems can handle the entire range of temperatures at which aircraft engines operate, from the lowest level at idle to the highest level during maximum throttle, throughout climb, cruising, and descent.

The sCO_2 waste heat recovery unit is designed based on the principles of a simple Brayton cycle which consists of the compressor (C), turbine (T), cooler, primary heat exchanger (PHX), and a recuperative heat exchanger (RHX). The cooler and PHX are directly connected to the aircraft engine. The following Figure 5 shows the schematics of an aircraft engine with a sCO_2 waste recovery unit (Vesely et al. 2022).

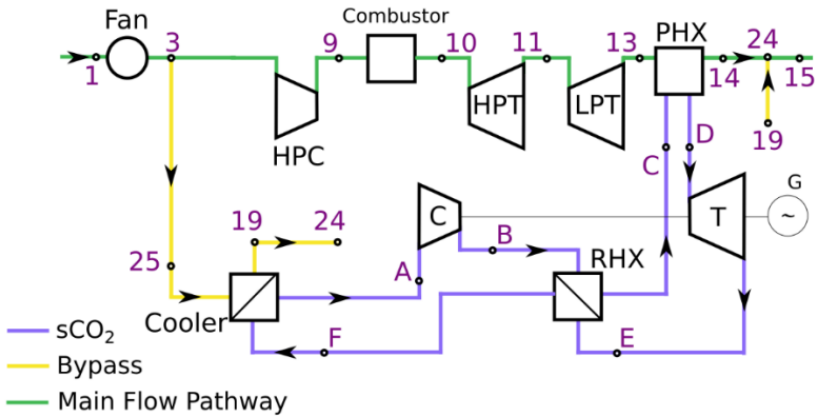

Figure 5 Schematics of an aircraft engine with sCO_2 waste recovery unit and recuperative heat exchanger (Vesely et al. 2022).

2.4 Seals in Aircraft Engine

One of the primary drivers of technological innovation in the aviation sector is the reduction of fuel consumption and carbon emissions, as well as the impact on the environment. There are also some more improvement scopes in aviation engines, such as airframe aerodynamics, engine nacelle flow aerodynamics, and weight reduction of

propulsion system. However, one of the most anticipated study fields in the next years is the decrease in airframe and engine construction weight. Reducing an aircraft's total weight improves engine efficiency, operational costs, and lifetime. Advanced sealing techniques have been demonstrated to provide the aviation sector with more efficient, lightweight, and cost-effective aircraft engines. Furthermore, developing a low leakage seal is 4 to 5 times less expensive than redesigning any other component of a jet engine. (B. Steinetz, Hendricks, and Munson 1999)

Performance is related to engine clearance. Fluid film sealing has an effect on annual energy savings by improving oil efficiency (Lawrence P. Ludwig and Bill 1980). In terms of engine bleed, if the fluid film sealing is reduced by 1%, engine bleeds give a 0.4 percent reduction in specific fuel consumption (Moore 1975). Refurbishing compressor seals not only reduces heat rate but also increases the power output of gas turbines (R. Chupp, Ghasripoor, and Moore 2002).

The key location of seals for the compressor and the turbine for industrial engines has been studied (Aksit et al. 2002)(Camatti and Vannini 2003). Figure 6 shows the location of the high-pressure compressor and turbine tip seal, interstage seal such as brush seal, and honeycomb seal.

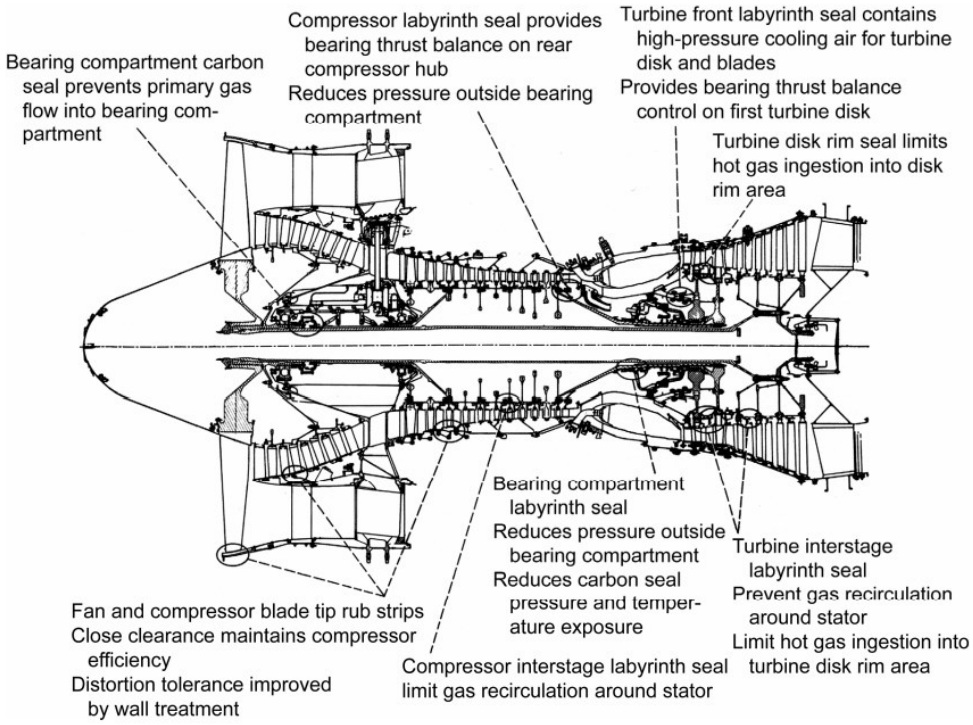

Figure 6 Aircraft engine seal and thermal restraint location(Bill and Ludwig 1980).

Currently, modern aircraft engines use a variety of seal designs and materials. Air-to-oil and air-to-air seals are the two main types of aircraft engine seals. Each seal has a distinct location and habitat in which to operate. For example, air-to-oil seals are employed in gearboxes and hydraulic cylinders to reduce oil loss under high-pressure conditions. (Shabbir, Garvey, and Dakka 2019) On the other hand, air-to-air seals are used in turbines and compressors to minimize the gas leakage from the system which eventually helps to increase the efficiency of the engine.(Ibrahim, Gillespie, and Garratt 2017) (I. P. Ludwig and Ludwig 1978)

In addition to that seals can be classified based on their dynamic and static characteristics. Figure 7 shows the classification of major seals that are used in aircraft engines.

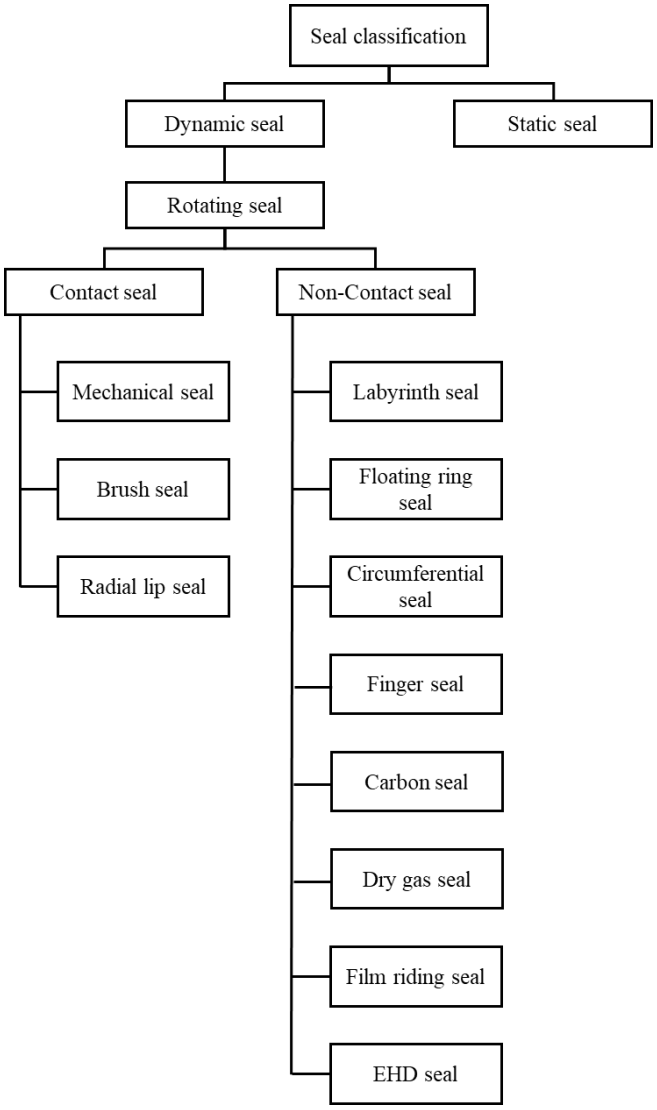

Figure 7 Aircraft engine seal classification

2.4.1 Static Seal

Static seals have been used in the steam-turbine packing ring segment end gaps, hot gas path junctions, and gas-turbine combustor junctions. Adjacent members usually have to withstand relative vibration with minimal or no wear or sealing loss. In order to regulate

parasitic leakage flows between turbine components, modern gas turbines need high-temperature, low-leakage, and compliant seals. Proper sealing enhances the main gas-path temperature profile in addition to increasing turbine power and efficiency (Aksit et al. 2002). Though an O-ring is a static seal, O, C, and E-type metallic seals are utilized as static seals in aircraft engines and comparable-type turbomachinery. Metallic cloth seals, static seals, are employed in high-temperature zones with rather large gaps. Another static seal used to improve structural integrity is the rope seal (R. E. Chupp et al. 2006a). Figure 8 shows the static seal location in a gas turbine.

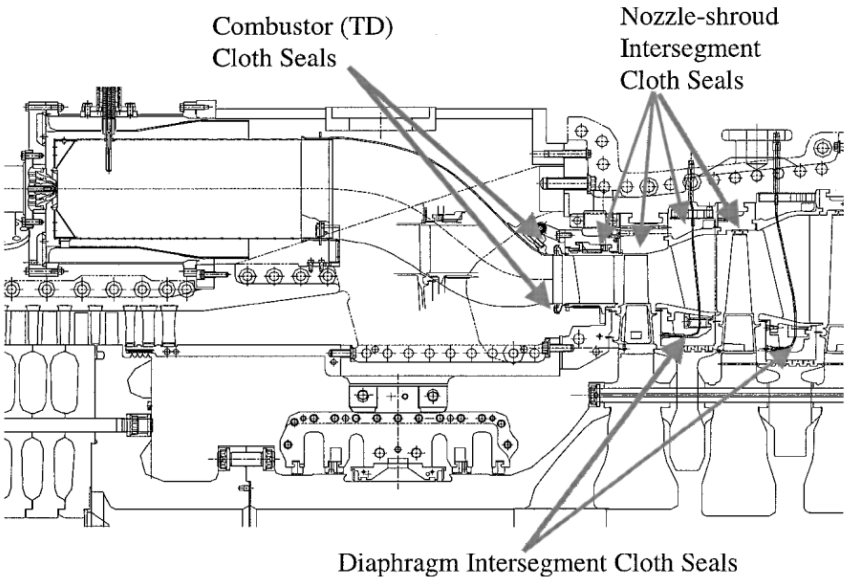

Figure 8 Advance static seal location (Aksit et al. 2002).

However, the most used static seal, the O-ring seal problem leads to dangerous acts. A significant leak, such as that of hydraulic fluid or lubricating oil, can cause major parts to fail, including the aero-engine and control units and bearings. The aircraft may be put at risk if escape leaking fluid catches fire. Adverse media or breakdown products near heated components (such as hydraulic fluid) have the potential to cause hazardous corrosion failures (Rossmann 2023).

2.4.2 Dynamic Seal

In linear, oscillating, and rotating motion applications, dynamic seals are the kind of seals that provide a barrier between fixed or moving surfaces. The functions of these seals include removing contaminants, applying pressure, and separating or holding fluids. Dynamic seals can be more crucial since they are more prone to wear and tear because of friction with one or two moving components. The following two groups comprise dynamic seals.

- Clearance Seals: Positive clearance seals are provided to prevent contact between mating surfaces.
- Contact Seals: These seals establish a sealed contact by applying pressure to the surface.

Tip sealing is considered one of the dynamic sealing systems because the blade tip leads to flow losses and instabilities. Improper sealing may reverse the flow domain and cause a surge in the compressor or fire. The revolving blade wears in abrasive seal materials during service. They are used on compressor casings, as well as gas and steam turbine casings, to reduce clearances to levels that are difficult to obtain mechanically(R. E. Chupp et al. 2006b).

2.4.2.1 Labyrinth Seal

Labyrinth seals and related sealing principles are widely used in turbomachinery and may be found in a wide range of designs. Straight, interlocking, slanted, stepped, and combinations are the most common configurations. Figure 9 shows the variations of the labyrinth seal.

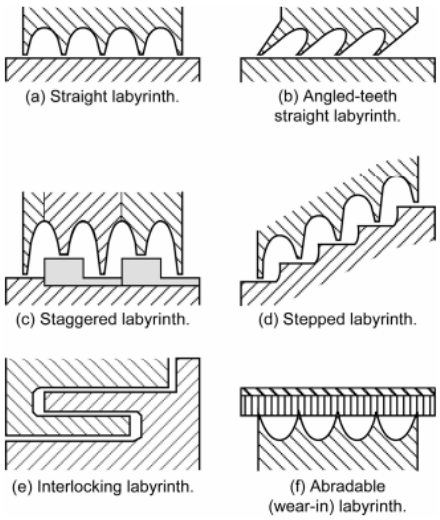

Figure 9 Types of labyrinth seal (Burcham 1979).

The labyrinth seal's popularity comes because of its simple design and longevity. In different conditions, the seal is capable of avoiding undesirable contact between the rotor and stator of the jet engine. This seal has a row of teeth that are oriented toward the rotating rotor. Pressure gradually decreases as the gas or liquid passes between the teeth, limiting leaking past the seal. Due to the nature of the seal design, the seal's ability to prevent leakage is highly reliant on several design elements. These elements are determined by shaft diameter, operating pressure, and speed. In general, the leakage rate is related to the spacing between teeth and inversely proportional to the number of teeth (Kim et al. 2019). Figure 10 shows the labyrinth seal schematics diagram in a gas turbine.

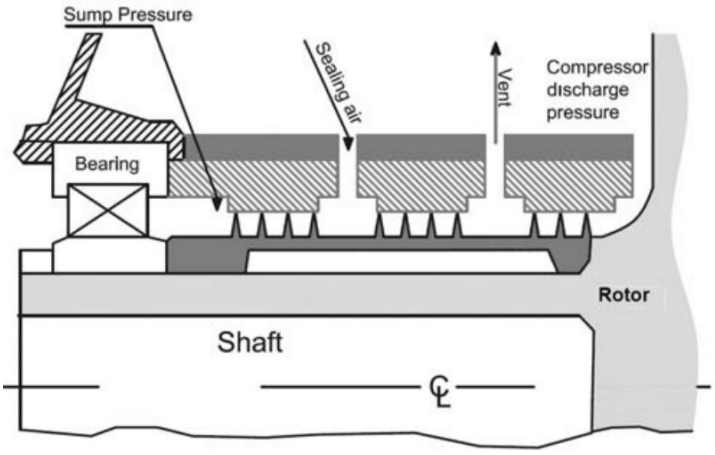

Figure 10 Schematics of labyrinth seal application (Aslan-zada, Mammadov, and Dohnal 2013).

(von Plehwe, Krug, and Bauer 2016)investigated oil leakage phenomenon through labyrinth seal by experimental setup and numerical analysis. In their study, it has been mentioned that minimum differential pressure is required to prevent oil leakage from the bearing chamber and critical differential pressure has been identified for various test setups. However, the result has been considered in engine ideal conditions and shaft misalignment, thermal distortion, and seal wear are not considered in this regard. Another labyrinth seal experimental setup has shown that by the increase of rotating speed, axial sealing air is constantly reduced, and the leakage coefficient increases (Li, Zhang, Lei, et al. 2019). Moreover, by the increase of clearance between the seal tooth tip and stator, tooth tip thickness, and pitch also increase the leakage coefficient. (Hühn et al. 2018) performed experimental and analytical analysis and mentioned that, at high operating temperatures, additional tensile stress is sufficient to initiate a hot crack in the labyrinth seal fin. The performance of the labyrinth seal mostly depends on the clearance between tooth tips and the opposing surface. Another drawback of labyrinth seal is response while dynamic loading

which eventually leads to the rotor-bearing instability system (Aslan-zada, Mammadov, and Dohnal 2013).

2.4.2.2 Floating Ring Seal

The floating ring seal is a form of labyrinth seal that may function with less leakage gap clearance than traditional labyrinth seals (Lynwander 1973). The floating seal can operate in high temperature and pressure zones with substantial vibration in the system. The seal has two rings, one is stationary, and the other is rotating. In the seal, a rotating carbon ring is enclosed in a stationary steel ring. To absorb the vibration, the ring slides on the rotor and maintains the clearance between the ring and the rotor (Li, Zhang, Huang, et al. 2019; L. P. Ludwig and Johnson 1974). Figure 11 shows the schematic of a floating ring seal with housing and shaft.

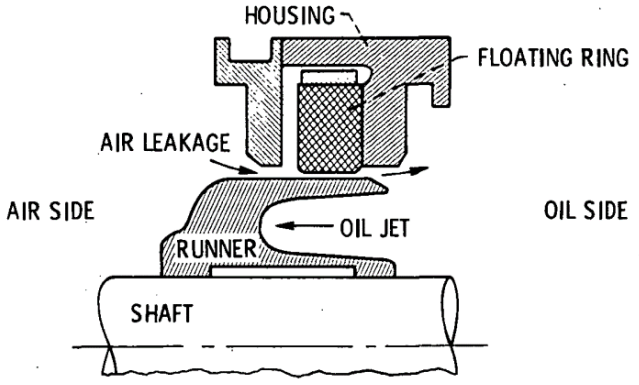

Figure 11 Schematics of a floating ring seal (L. P. Ludwig and Johnson 1974)

2.4.2.3 Brush Seal

The brush seal is the first simple, practical alternative to the finned labyrinth seal that provides significant performance gains (Ferguson 1988). Brush seal has reduced leakage compared to labyrinth seal, shaft diameter can be varied, compact and provide stable leakage

characteristics than labyrinth seal (R. E. Chupp et al. 2006b). The following Figure 12 shows the schematics of a brush seal.

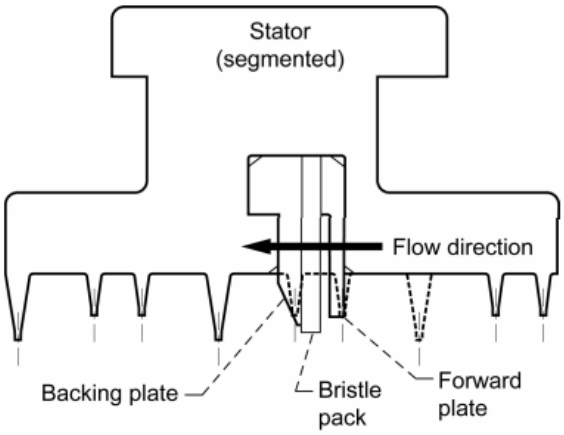

Figure 12 Schematics of a brush seal and geometry features (Dinc et al. 2001)

The brush seal has three basic components. The brushes, which are tangentially aligned with the rotor, are one example. This type of alignment allows the seal to move in response to vibration and heat loads, reducing leakage rates. A backing plate positioned axially supports another component known as the bristle pack. The backing plate avoids the bending of the bristle pack (Pröstler 2002).

Due to the direct contact with the rotor, brush seals provide better sealing than a comparable labyrinth seal. However, because of this contact, brush seals experience significant wear over time. As the bristle gets worn down, the overall effectiveness of the brush seal is decreased (Ferguson 1988). For example, initial wear-in causes a considerable rise in the leakage flow (R. E. Chupp and Nelson 1993). When there is a contact between two parts, as a product heat is produced which leads to extreme wear and grinding down the bristle and rotor dynamics that are disrupted as a result of severe thermal heating (Dinc et al. 2001). A typical brush seal is compatible with 1300 °F or less and for 1000 ft/s surface speed

or less, which falls short of what is required for a contemporary aircraft engine to operate (Liu 2009).

2.4.2.4 Circumferential Seal

The circumferential seal is for minimizing the leakage of gas or oil by maintaining the clearance between the circumferential ring and the rotating shaft. However, the operating pressure for the circumferential seal is lower than the other seal(L. P. Ludwig and Johnson 1974).

Carbon-graphite segments are used for circumferential main shaft seal rings. They are designed to fit with little space in slots within the fixed housing. Three 120° carbon-graphite segments are held under strain against a ceramic or hard metal covering on the revolving shaft via a "garter" spring (L. P. Ludwig and Johnson 1974). Figure 13 shows the circumferential seal with the segmented ring.

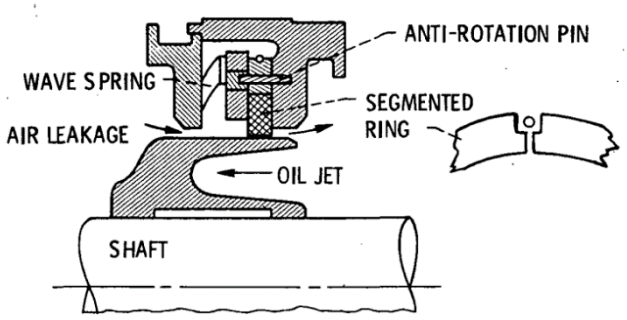

Figure 13 Schematics of a circumferential segmented seal (L. P. Ludwig and Johnson 1974)

2.4.2.5 Finger Seal

Finger seals are a type of compliant seal that can be installed on fixed components as well as on moving ones. They are part of the same category of seals as brush seals, foil seals, and leaf seals. Finger seal's potential lifting capability helps maintain seal integrity

and significantly reduces wear, resulting in a longer lifespan compared to brush seals and labyrinth seals. Furthermore, the seal has lower manufacturing cost with better thermal adaptability, which establishes its application in various jet engines(Zhao, Su, and Chen 2020). Figure 14 shows the axial structure of the finger seal and finger element.

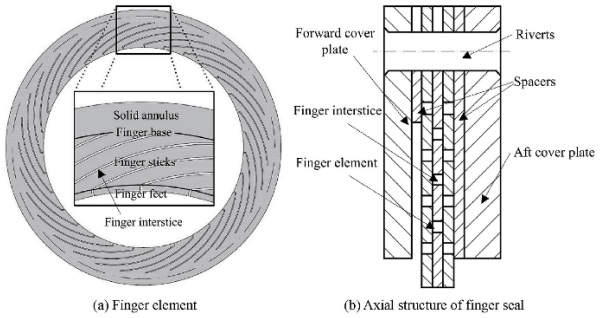

Figure 14 Schematics of a finger seal (Zhao, Su, and Chen 2020)

The first contacting type finger seal was introduced in 1991 as an alternative to brush seal. The seal is made up of annulus-shaped laminates arranged in numerous circumferential layers in a staggered pattern. The seal is made of carbon or composite metal. Since the seal makes contact with the rotor, Arora introduced a novel non-contacting padded finger seal that operates based on hydrodynamic lift. This force is essential to prevent the seal from making contact with the rotor (Bidkar et al. 2017; Alastair Cameron 1996).

2.4.2.6 Face Seal

Face seals are mechanical seals. They are pressure-balanced contact or self-acting seals. The primary ring (stator) or nosepiece, seat or runner (rotor), spring or bellows preloaded assembly, garter or retainer springs, secondary seal, and housing are the main components. The following picture shows the schematics of the face seal.

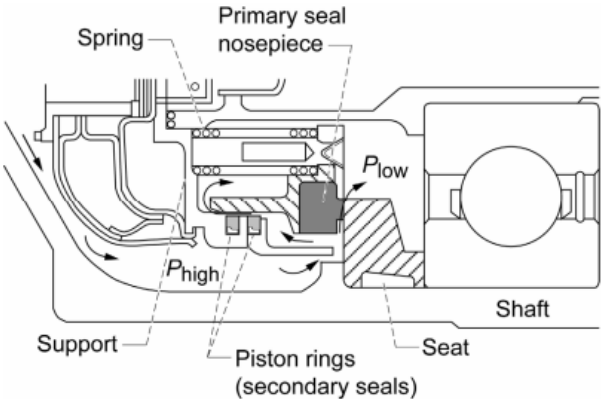

Figure 15 Schematics of a positive contact face seal (Loomis 1984)

In order to enable a rotating element to pass through a sealed container, the face seal utilizes both stiff and flexible parts that glide over one another while maintaining contact at the sealing interface. This seal design can reliably control leakage in operational conditions where pressure is less than 150psi and rotational speeds are up to 475 ft/s. For a mechanical face seal to operate, an adequate state of lubrication is needed. If a satisfactory state cannot be achieved, the seal will wear out our destroyed by the thermal mechanism (Liu 2009).

2.4.2.7 Carbon Seal

In 1967, NASA introduced carbon seals(Burcham 1967). The use of a carbon seal in the bearing chamber is an efficient solution for preventing oil leaks. The leakage properties of carbon seals lie between those of labyrinth seals and mechanical seals(Boston et al. 2014). The carbon seal typically consists of several carbon segments, a circumferential spring, an axial spring, a baffle, and a snap ring(LI et al. 2022). Figure 16 shows the carbon ring seal with a garter spring.

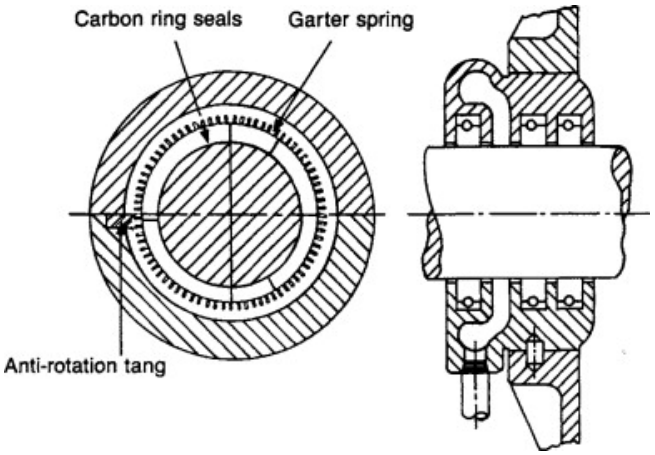

Figure 16 Schematics carbon seal ("Steam Turbines and Turboexpanders" 1997)

2.4.2.8 Lip Seal

Lip seal is used in turbomachinery to restrain the solid and liquid leakage at low pressure. The seal is used for rotating the shaft and attached to a mechanical housing. The seal leaf is made of synthetic rubber and a garter spring controls the seal movement. Although the seal has a basic structure, it has remarkable sealing performance. The lip seal relies on the formation of a thin layer of oil between the lip and the rotating shaft to create an effective seal (Stakenborg 1988).

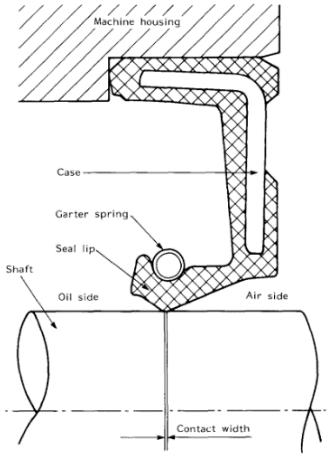

Figure 17 Schematics lip seal (Stakenborg 1988)

2.4.2.9 Dry Gas Seal

In 1970, the dry gas seal was introduced to overcome the complexity of the floating ring seal. The seal is simple in design and requires less support than the other seals. The seal has two rings, the rotating ring has a grooved pattern to enhance the sealing performance, and the stationary ring is attached to the spring retainer assembly by a spring. There is little or no leakage when the faces are in contact (Cich et al. 2020). Figure 18 shows the dry gas seal with spring retainer assembly and dynamic sealing element.

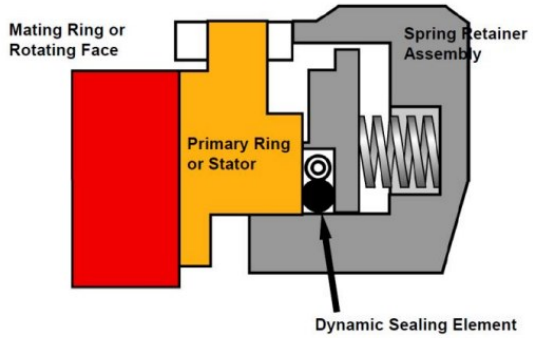

Figure 18 Schematics of dry gas seal (Cich et al. 2020)

2.4.2.10 Film Riding Seal

Film riding seal was first introduced in 2010, based on pressure-actuated leaf seal theory. In the leaf seal, multiple frusto-conical layers are placed at high pressure side, supported by seal members and the back ring. These elements are connected to the stator. And there is a big clearance between the seal and shaft in cold conditions. At operating conditions, there will be a pressure difference between the seal's outward side and inward side. Small seal clearance at operating conditions provides the required sealing performance. After the unit shuts down the seal goes back to its original position (Grondahl and Dudley 2010).

For film riding seals, can maintain the seal clearance in every operating condition. This seal introduces segmented runners which can balance hydrostatic force and hydrodynamic lift and maintain small clearance with low leakage(Grondahl and Dudley 2010).

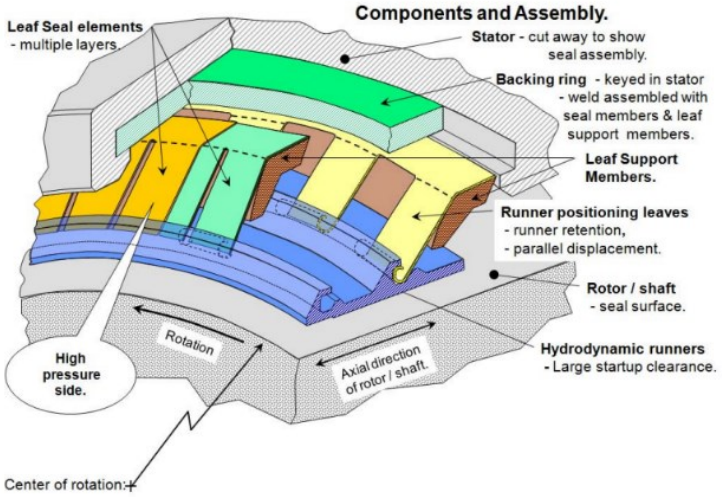

Figure 19 Schematics of the conceptual design of film riding seal (Grondahl and Dudley 2010)

CHAPTER 3

METHODOLOGY

The primary goal of this study is to investigate the behavior of the multistage EHD seal in relation to airplane engine's sCO_2 waste heat recovery unit (Lyathakula, Cesmeci, Hassan, et al. 2022b; Lyathakula, Cesmeci, DeMond, et al. 2022). The seal design idea and its numerical analysis must be explained in depth in order to achieve this. Thus, a comprehensive explanation of the seal design, an analytical method for supporting it, and a numerical analysis have all been provided in this chapter.

3.1 Seal Concept

The EHD seal concept is based on proven elastohydrodynamic lubrication theory (H. Xu and Lei 1994; H. P. Xu, Wong, and Zhang 1999; Wong, Xu, and Zhang 1997). The EHD seal design has three steps. Each step is made of similar components. The operating principle of the proposed multistage EHD seal is illustrated in the following Figure 20 & Figure 21.

At the starting position, the seal is attached to the back ring and sits off the rotor maintaining the clearance h. Once the system started, the pressure P_1 gradually increased and became greater than P_2. This working pressure exerts consistent stress on the seal's top and causes the clearance to decrease linearly until a throat is formed. The seal may expect to bend all the way close the flow the clearance and restrict the flow. However, the clearance will never be zero since the upstream pressure P_1 is always greater than the downstream pressure P_2. The throat will be forced open by the pressure differential, allowing the seal and rotor to be separated by the smallest amount of clearance (Henry et al. 2023; Islam et al. 2023; Lyathakula et al. 2023; Hassan, Xu, Islam, Cesmeci, et al. 2024; Hassan, Xu, Islam,

and Cesmeci Sevki 2024; Hassan, Xu, Cesmeci, Wasif Hasan, et al. 2024). Leaks that get past the first seal then move on to the second step, where the same thing happens again. Physics-based computer simulation will be used to test this theory.

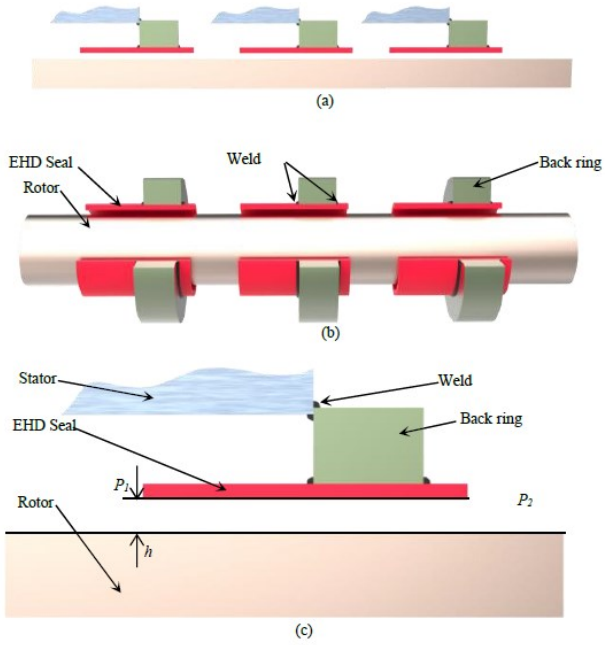

Figure 20 Multistage EHD seal in cold condition (a) 2D schematic diagram, (b) 3D schematic diagram, and (c) cross-sectional of EHD seal– parts are not drawn to scale.

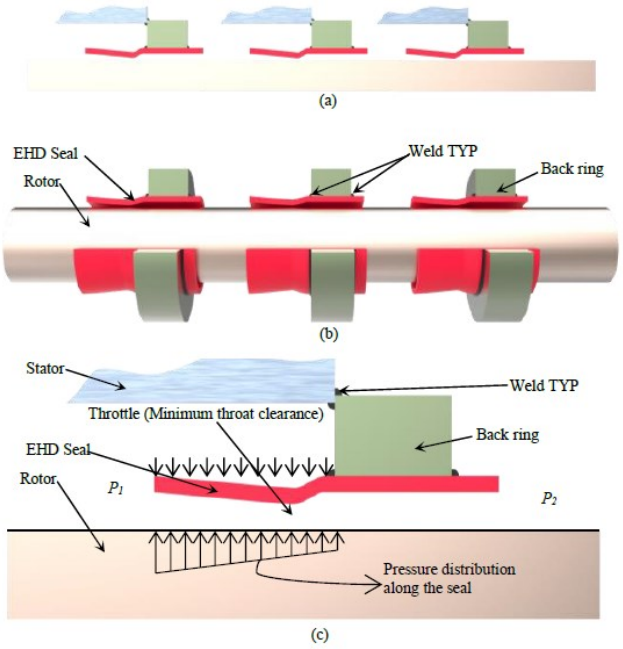

Figure 21 Multistage EHD seal in operating condition (a) 2D schematic diagram, (b) 3D schematic diagram, and (c) close-up view of EHD seal– parts are not drawn to scale.

During the throttling process, the pressure will decrease to its minimum level. This will result in the formation of vena contracta (Islam et al. 2023). From the vena contracta concept, following the reduction in flow rate, the pressure will partially regain its original level, which is dependent upon the difference in pressure between the seals. The vena contracta effect is shown in the following Figure 22. The occurrence will be discussed in the result section.

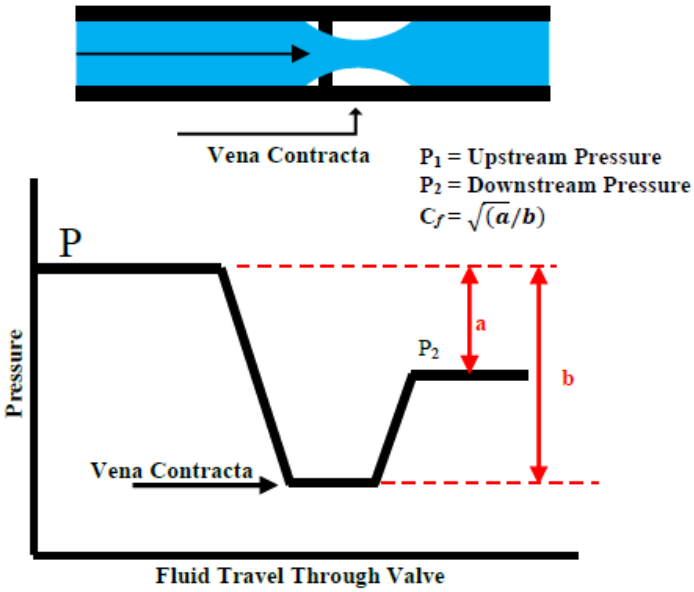

Figure 22 Vena contracta effect.

3.2 Numerical methodology

The EHD seal theory is based on the elastohydrodynamic lubrication theory and is generally studied with the Reynolds equation (Lyathakula, Cesmeci, Hassan, et al. 2022a; Cesmeci et al. 2022; Gong et al. 2016; Cesmeci et al. 2021). The flow field inside the clearance zone was subjected to the Reynolds equation. The following is the Reynolds equation in cartesian coordinates.

$$\frac{\partial}{\partial x}\left(\frac{\rho h^3}{\mu}\frac{\partial P}{\partial x}\right)+\frac{\partial}{\partial z}\left(\frac{\rho h^3}{\mu}\frac{\partial P}{\partial x}\right)=6\frac{\partial(\rho u h)}{\partial x}+6\frac{\partial(\rho v H)}{\partial z}+12\frac{d(\rho h)}{\partial t} \quad (1)$$

In equation 1, x and z represent the axial and vertical directions, P is the pressure, h is the film thickness, μ is the dynamic viscosity of the fluid, ρ is the density of the fluid, and t is the time.

There are restricted situations in which the Reynolds equation can be applied. These assumptions include steady, laminar, and incompressible flow. The precision of this analytical procedure is compromised when certain criteria are not satisfied. Due to large pressure differentials and small clearances, the recommended seal design may induce a sonic state. As a result, the Reynolds equation cannot accurately and completely characterize the flow conditions on its own(Cesmeci et al. 2023). Using CFD software and tools is a commonly available analytical method that works efficiently for EHD lubrication studies (Feldermann, Neumann, and Jacobs 2017). COMSOL Multiphysics software, an advanced CFD software supplier, was used to simulate the fully coupled fluid-structure interaction. In the following Figure 23, it shows the solution approach that was followed in COMSOL Multiphysics.

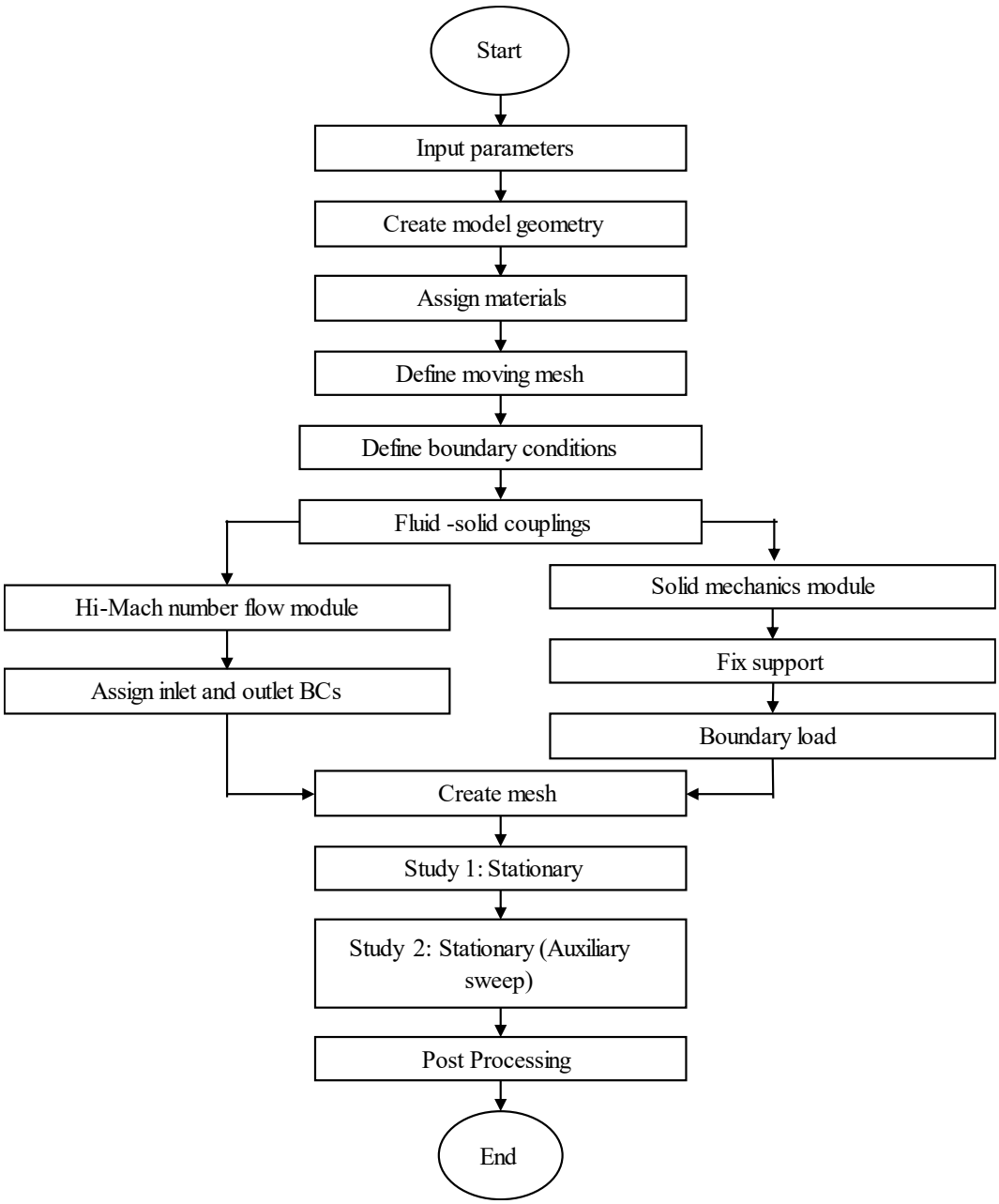

Figure 23 Simulations steps in COMSOL Multiphysics

In the simulations, the pressure field was solved in the flow domain, then the pressure was applied to the seal as a boundary load. The solid domain generated seal displacement and was sent back to the flow domain until the convergence happened. Figure 24 shows the interaction process in COMSOL Multiphysics.

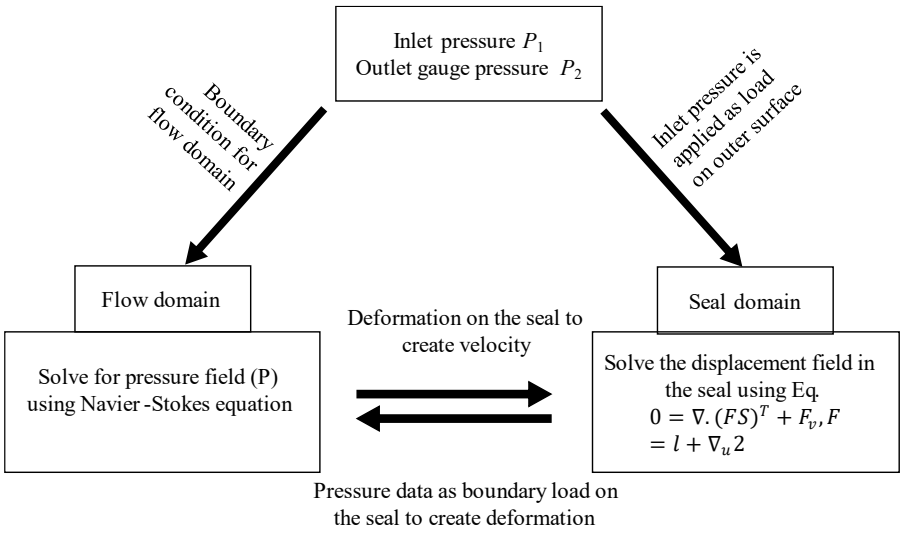

Figure 24 Interaction process in COMSOL Multiphysics.

3.2.1 Model Geometry and Mesh

The 2D geometry was created in COMSOL for numerical analysis. The single sealing procedure in detail is shown in Figure 25 below, along with precise dimensions. Additionally, Figure 26 displays the mesh that corresponds to the multistage geometry that COMSOL created.

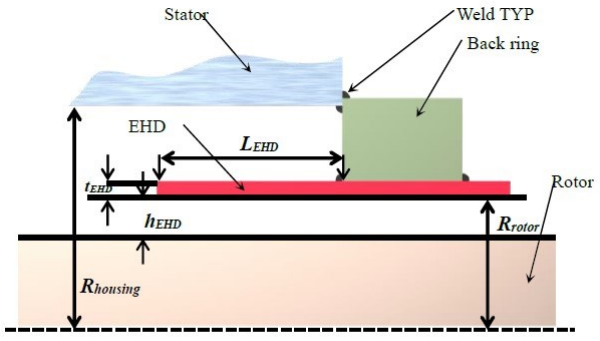

Figure 25 Important geometric dimensions of the EHD seal −parts are not drawn to scale.

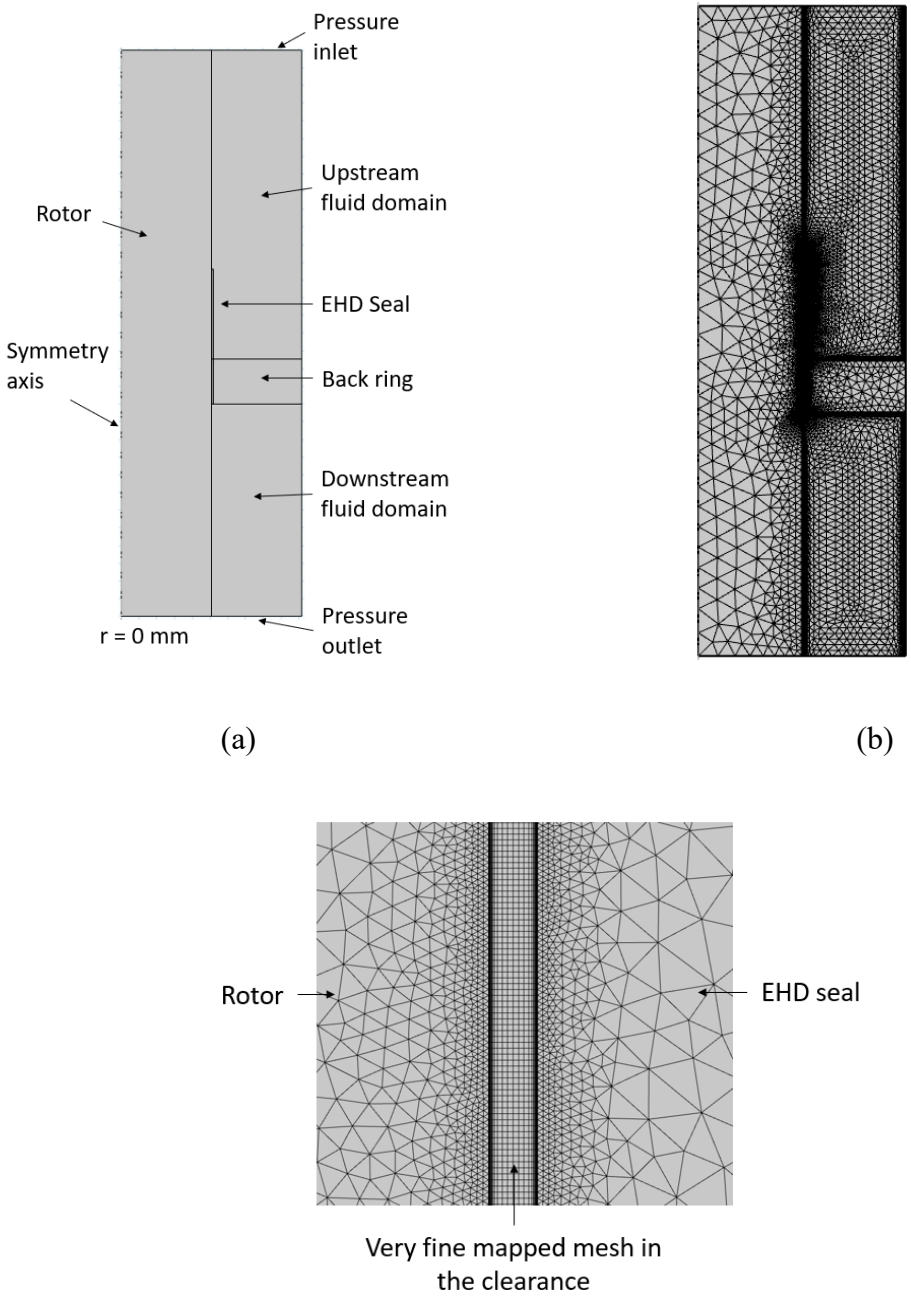

Figure 26 EHD (a) model geometry with its main components, (b) generated mesh, and (c) close view of the mapped mesh in the clearance.

To optimize efficiency, the simulations were run using a 2D axisymmetric model. All of the solid and fluid domains in the model were meshed using triangle components, except the clearing regions. Rectangular components were used to mesh this section of the model. Besides the "wall functions" of the solver, boundary layers were applied to all fluid boundaries in order to capture the very viscous effects close to the walls. 123,609 domain elements and 5,801 boundary elements made up the whole mesh when the maximum element size in the clearance was set to 0.025 mm.

3.2.2 Material

All the major components of the seal design were constructed out of structural steel. Air as an ideal gas was utilized for all fluid components in the simulation. The steel was described as an isotropic, linearly elastic substance with v=0.30, E=200 GPa, and ρ=7,850 kg/m^3. The density of ideal gas is defined by the ideal gas equation of state, while its thermal conductivity and dynamic viscosity were defined by Sutherland's Law.

Thermal conductivity:

$$k = k_{ref}\left(\frac{T}{T_{k,ref}}\right)^{3/2}\frac{T_{k,ref}+S_k}{T+S_k} \tag{2}$$

where T is the temperature, $k_{\text{ref}} = 0.0241\,\text{W/m}\cdot\text{K}$, and $T_{k,\text{ref}} = 273\text{ K}, S_k = 194\text{ K}$.

Dynamic viscosity:

$$\mu = \mu_{\text{ref}}\left(\frac{T}{T_{\mu,\text{ref}}}\right)^{3/2}\frac{T_{\mu,\text{ref}}+S_\mu}{T+S_\mu} \tag{3}$$

In the above equation, μ represents the dynamic viscosity and $\mu_{\text{ref}} = 1.716e^{-5}$ Pa $\cdot$ s, and $T_{\mu,\text{ref}} = 273\text{ K}, S_\mu = 111\text{ K}$.

3.2.3 Computational Method

Since compressible and turbulent effects are more likely to occur in the fluid domain's clearance and downstream flow zones, the High Ma Number Flow (HMNF) module was chosen. The RANS, k–ϵ, and Kays– Crawford models were chosen as the turbulence model type, turbulence model, and heat transport turbulence model, respectively. The equations used in the flow domain are as follows:

Steady continuity:

$$\nabla \cdot (\rho u) = 0 \tag{4}$$

Steady Navier-Stokes:

$$\rho(u \cdot \nabla)u = \nabla \cdot [-pI + K] + F \tag{5}$$

Turbulence model:

$$K = (u + \mu_T)(\nabla u + (\nabla u)^T) - \frac{2}{3}(u + u_T)(\nabla \cdot u)I - \frac{2}{3}\rho k I \tag{6}$$

$$\rho(u \cdot \nabla)k = \nabla \cdot \left[\left(\mu + \frac{\mu_T}{\sigma_k}\right)\nabla k\right] + P_k - \rho\epsilon \tag{7}$$

Steady energy equation:

$$\rho C_p u \cdot \nabla T + \nabla \cdot q = Q \tag{8}$$

The variables used in the equation are as follows: ∇represents the gradient operator, ρ denotes the density, u represents the velocity vector, p stands for pressure, τ represents the viscous stress tensor, F represents the volume force vector, Cp represents the specific heat capacity at constant pressure, T represents the absolute temperature, q represents the heat flux vector, Q contains the heat sources, S represents the strain-rate tensor, K represents the

turbulent kinetic energy, *k* represents the Thermal Conductivity, *ep* represents the turbulent dissipation rate, μ represents the dynamic viscosity, μ_T represents the eddy viscosity, and $C_{\epsilon 1}$, $C_{\epsilon 2}$, σ_ϵ, and σ_k are adjustable constants. The variables *u* (and its components u,v,w), *p, k, ep*, and *T* are the dependent variables in the equations mentioned above.

Solid domain:

$$0 = \nabla \cdot (FS)^T + F_V, \quad F = l + \nabla u2 \tag{9}$$

Here, *FS* is the 1st Piola-Kirchhoff stress sensor, whereas *l* is the unit tensor, *u*2 represents the displacement and F_v is the force vector.

To validate the simulation methods, the analytical answers were compared to the simulation findings for one-way coupling. Equation 10 yields the absolute pressure value which has been used in the simulation for the initial value.

$$P_{\text{analytical}} = \sqrt{P_0^2 + \frac{(P_e^2 - P_0^2)x}{L_{\text{seal}}}} \tag{10}$$

3.2.4 Boundary Condition

The boundary condition was set for the inlet pressure P_1 for the waste heat recovery unit's turbine to allow for observation of the seal's complete operational range, which spans from 0.1 MPa to 19 MPa. The outlet pressure was determined to be atmospheric pressure.

The seal geometry was a single solid edge geometry, specifically identified as a solid wall with well-defined limitations within the fluid domain. The EHD seal domain is allowed to undergo deformation. All the solid and fluid domain wall connections were thermally insulated. For the analysis, the energy equation was only solved in the fluid domain. As a result, there is no conjugated heat transfer between the solid and fluid domains. As stated

previously, the solid and fluid domains were fully linked when boundary loading was applied to the edges of the seal geometry.

3.3 Mesh Independence

The nonlinear elements in the Navier-Stokes momentum and energy equations make solving viscous flow problems computationally difficult. Meshes are used to describe a collection of finite volume components that are utilized to depict the issue in computational fluid dynamics. Section 3.2.1 illustrates the total number of boundary domains and elements to discretize the problem in this study. To enhance the mesh design and ensure computational efficiency, several criteria are evaluated for independence validation.

3.3.1 Mesh Sequence

In the study, the user-controlled mesh was used for the mesh sequence. In general, the mesh was calibrated for general physics, and coarse mesh was used for meshing. However, for each seal's outlet domain, the mesh was calibrated for fluid dynamics and the mesh type was normal. For the most sophisticated region, the clearance region, an extremely fine mesh type was used.

3.3.2 Mesh Size

The geometry was divided into multiple domains and each domain has a different sizing. For the seal fixed end, the maximum element size was 19.2 mm, and the minimum element size was 0.0862 mm. However, for each seal's outlet domain, the maximum element size was 2.29 mm, and the minimum element size was 0.102 mm. In the study, seal clearance is more sophisticated than other domains. A detailed mapped mesh was applied to the clearance section. The clearance section was distributed into 600 elements along with seal length and 10 elements along with the clearance height.

3.3.3 Independence Analysis

For mesh independence analysis, a total of six consecutive models were analyzed. In the first three model's domains, the mesh was set for coarser, coarse, and normal mesh respectively. Later user-defined mesh size was used considering the extremely fine mesh type. And leakage rate was also observed with an increment of distribution in the clearance region. In the following graph, the leakage rate was plotted against the element number.

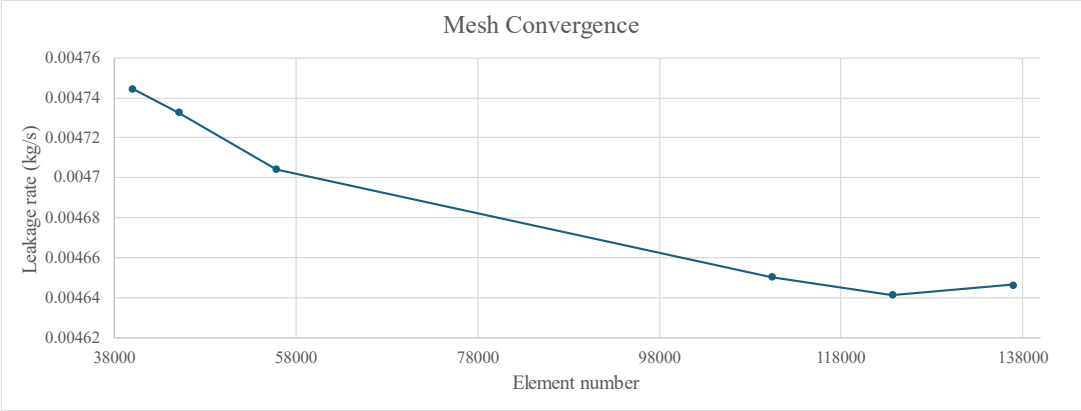

Figure 27 Mesh independency validation graph.

CHAPTER 4

RESULT AND DISCUSSIONS

The primary objective of this work was to verify the validity of the EHD seal hypothesis using physics-based computational models. Therefore, we initiate the process by creating deformation on the EHD seal. The simulations employ the geometrical and material properties stated in Table 1. The geometry and material properties are represented in a simple form for the waste heat recovery unit's turbine.

Table 1 Geometric and fluid properties for the analysis

Property/Parameter	**Value**
Rotor radius	25.4 mm
EHD seal thickness	0.25 mm
Seal clearance height	0.025 mm
EHD seal length	25.4 mm
Distance between the seals	38.10 mm
Young's modulus	200 GPa
Poison's ratio	0.30
Density	$7{,}850\ \mathrm{kg/m^3}$
Working fluid	Air
Gas constant	0.287 kJ/kg·K

Figure 28 illustrates the distribution of the pressure on the lower edge of the seal geometry. The results are extracted from analytical modeling and simulation. Both results

coincide with each other, which validates the simulation methodology. In terms of two-way coupling, it is difficult to solve with an analytical model due to the presence of high compressible flow in the clearance region. Therefore, the numerical model is solved with a High Mach number flow module and solid mechanics module in COMSOL.

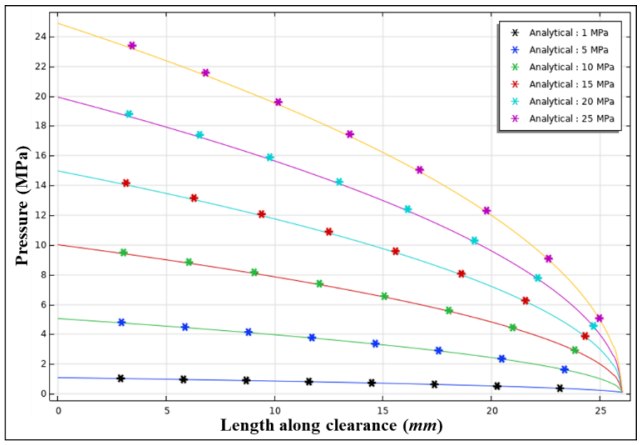

Figure 28 Comparison of analytical and numerical results for pressure field for the one-way coupling.

In Figure 29, the pressure distribution on the top edge is equally distributed, whereas the pressure distribution on the bottom edge decreases linearly. The combined impact of these two stresses leads to a seal distortion, as seen in Figure 28. The endpoints of the curve shown in Figure 27 correspond to the tip and base of the EHD seal. It is evident that a neck is developing toward the base of the seal, as anticipated. Figure 29 displays the seal displacement field for enhanced visual examination. Figure 30 and Figure 31 show a maximum deformation of approximately 0.0026 mm, corresponding to a minimum throat height of 0.0474 mm.

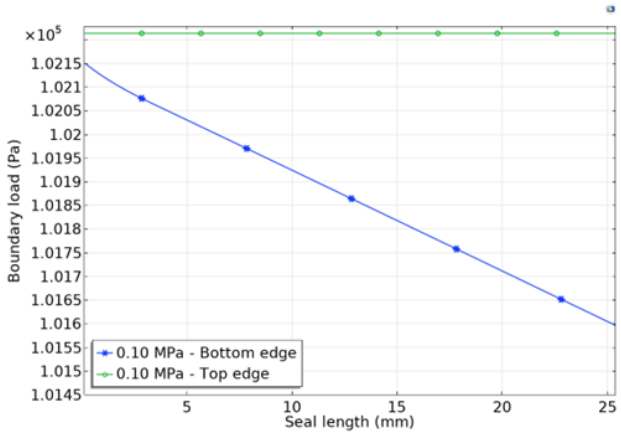

Figure 29 Uniform boundary load on the top and decaying load on the bottom of the seal.

Figure 30 shows the throating effect of the seal at an inlet pressure of 10 MPa. However, this measurement was conducted at a static intake pressure. As the intake pressure rises, the throat height gradually decreases to its minimum feasible height. As explained in Section 3.1, the minimum throat gap never approaches zero because, at that point, the pressure differential across the throat will exert a force that prevents it from closing completely. The following Figure 30 also demonstrates the minimum distance after the throating effect.

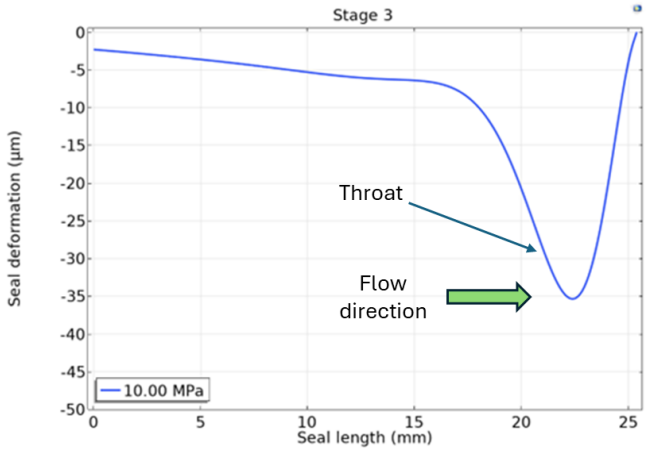

Figure 30 Deformation at the third stage at 10 MPa.

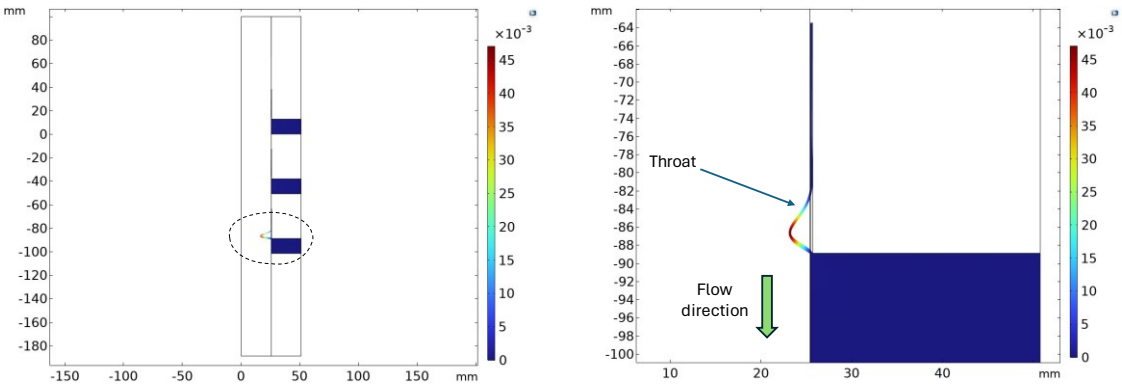

(a) (b)

Figure 31 (a) Maximum deformation of the multistage seal system at 19 MPa (b) magnified visualization.

Figure 32 illustrates that seal deformation has occurred at each level. However, during the third stage, the largest deformation occurred as a result of significant pressure differences.

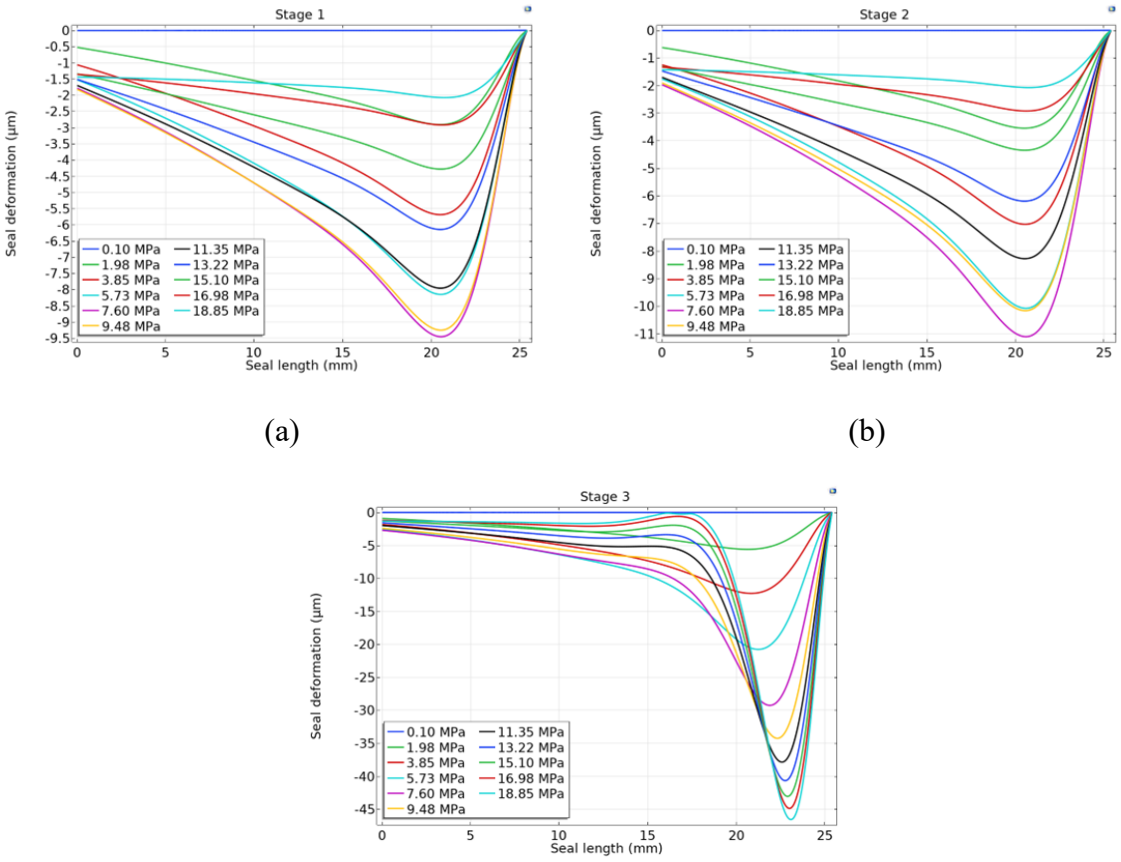

Figure 32 Deformation of seal at inlet pressure 0.1 MPa to 19.0 MPa; (a) stage 1 (b) stage 2 (c) stage 3.

The results presented in Figure 32, including pressure, temperature, density, and dynamic viscosity, align with our expectations based on the ideal gas equation and Sutherland's Law as stated in Section 3.2.2. The vena contracta effect, which was addressed in Section 3.1, is readily evident in Figure 33a.

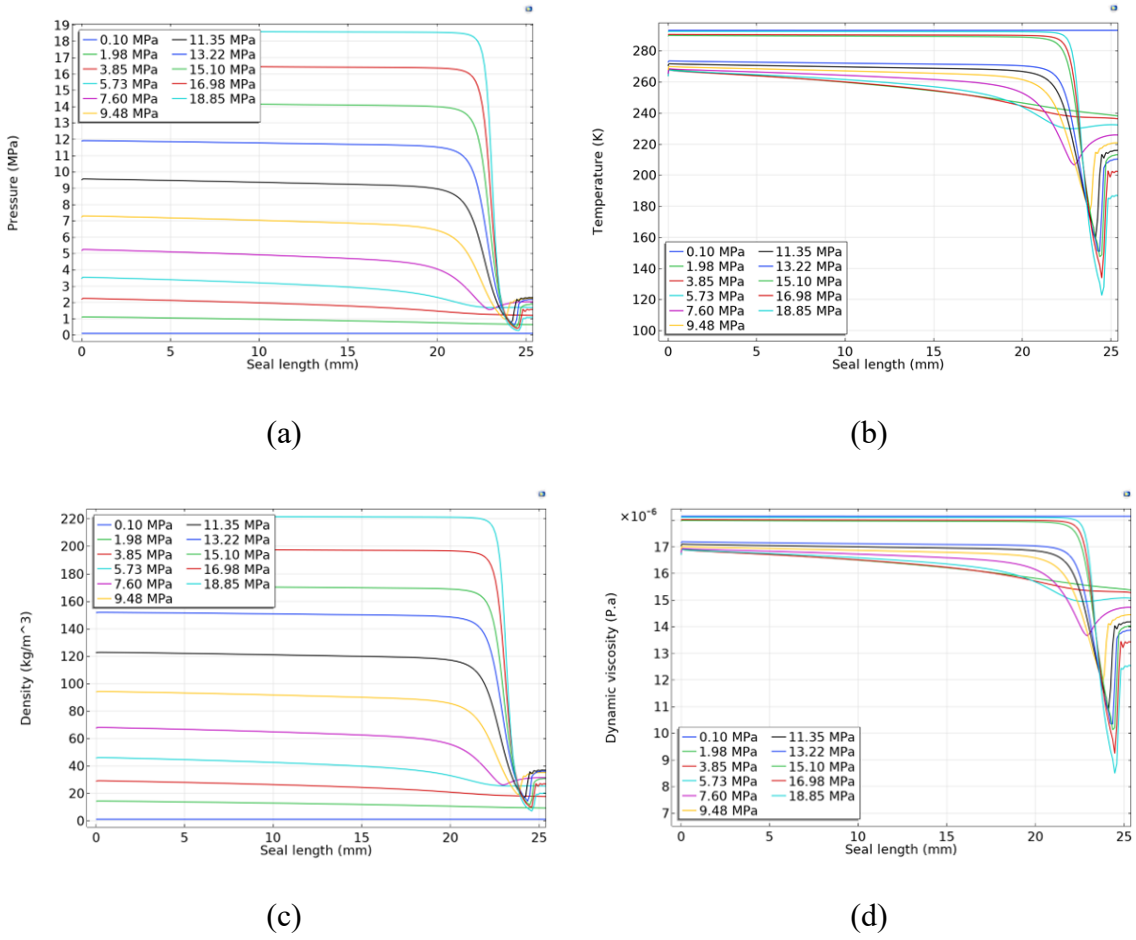

(a) (b)

(c) (d)

Figure 33 Parameters after the clearance (a) Pressure (b) temperature (c) density (d) dynamic viscosity.

Due to the pressure differences, the pressure value decreases along the seal and causes a throating effect adjacent to the fixed support of the seal. The throating effect introduces highly compressible flow at the clearance region. The highly compressible flow expands after the clearance region and flow velocity reaches supersonic condition. Figure 34 illustrates the compressible flow at the throat region and supersonic condition after the clearance region.

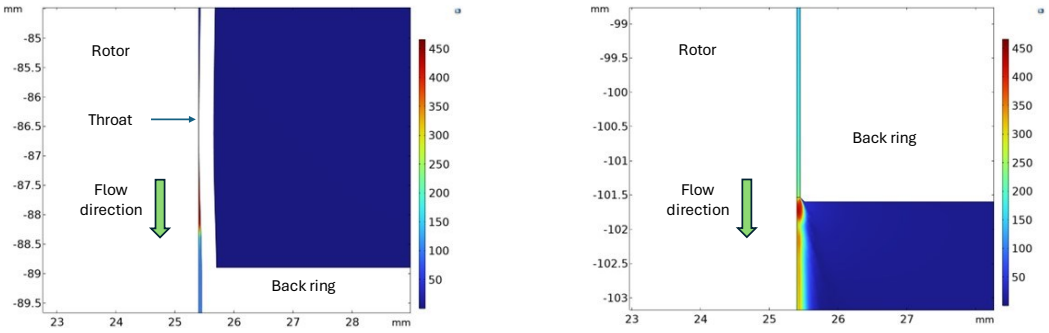

(a) (b)

Figure 34 Flow velocity at P_1 = 19 MPa (a) high compressible flow at throat region; (b) supersonic condition after clearance region.

Finally, the seal leakage rate across the whole range of operations is provided in Figure 35. In Figure 35, the leakage curve follows a quadratic pattern for the geometry, if the operating pressure range is up to 19 MPa. In this case, the leakage rate reaches its maximum at P_1 = 11 MPa before declining. The behavior of the EHD seal might be useful in high-pressure applications, such as sCO_2 waste heat recovery unit for aircraft engines. However, it is important to note that the mentioned leakage rates are exclusively for the particular geometric and material characteristics. An optimization study is still in progress to achieve the quadratic pattern for the lower pressure range as well.

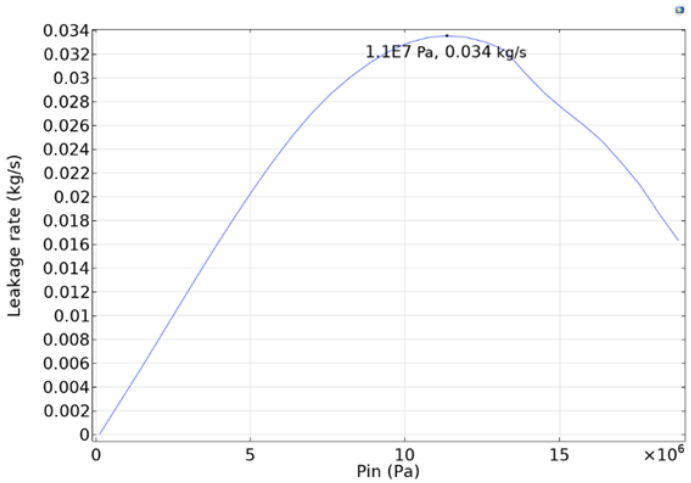

Figure 35 Leakage rate for pressure range 0.1 MPa to 19 MPa

CHAPTER 5

CONCLUSIONS AND FUTURE WORK

This study focuses on the proof-of-concept of a multistage electrohydrodynamic (EHD) seal for sCO_2 waste heat recovery unit for an aircraft engine. The key findings of this study can be listed as follows:

- The results indicated that the leakage can be successfully throttled by using a multi-stage EHD seal.
- While the first and second stages aided the leakage reduction, much of the leakage reduction occurred in the last stage. This is because the pressure built up in the last chamber.
- The leakage rate increased to 0.034 kg/s at 11 MPa before reducing to 0.016 kg/s at 19 MPa.
- The leakage can be controlled further by tailoring the material and geometric properties of the seals in each stage according to the design requirements.
- The proposed seal is not limited to the sCO_2 waste heat recovery unit for an aircraft engine and can also be used in air-breathing jet engines to minimize leakage and boost cycle efficiency.
- Although the proposed seal design was targeted for sCO_2 waste heat recovery unit for an aircraft engine application, it could also be used for other types of working fluids such as water and oil. Thus, it could have a long-lasting impact on the oil and gas industry.

5.1 Future Work

In the future, an analysis must be conducted taking into account the properties of the actual working fluid, rather than assuming it behaves like an ideal gas, and an optimization study will be conducted considering the material properties and geometry to achieve the required sealing behavior. In addition to the optimization study, a parametric study will also be conducted. A separate study will also be conducted for only aircraft engines by tailoring the seal design. A detailed comparative analysis will be conducted considering different boundary conditions and different regions in an aircraft engine. Conjugated heat transfer analysis will be implemented due to its potential impact on the clearance. One of the next aspects of this investigation is doing 3D simulations using a rotating rotor and considering eccentricity.

REFERENCES

Ahn, Yoonhan, Seong Jun Bae, Minseok Kim, Seong Kuk Cho, Seungjoon Baik, Jeong Ik Lee, and Jae Eun Cha. 2015. "Review of Supercritical CO2 Power Cycle Technology and Current Status of Research and Development." *Nuclear Engineering and Technology* 47 (6): 647–61. https://doi.org/10.1016/J.NET.2015.06.009.

Aksit, Mahmut F., Raymond E. Chupp, O. Saim Dinc, and Mehmet Demiroglu. 2002. "Advanced Seals for Industrial Turbine Applications: Design Approach and Static Seal Development." *Journal of Propulsion and Power* 18 (6): 1254–59. https://doi.org/10.2514/2.6060.

Alastair Cameron, by. 1996. "Noncontacting Finger Seal with Hydrodynamic Foot Portion." *CRC Handbook of Lubrication* 435 (73): 154–55.

Aslan-zada, Farhad E., Vugar A. Mammadov, and Fadi Dohnal. 2013. "Brush Seals and Labyrinth Seals in Gas Turbine Applications." *Proceedings of the Institution of Mechanical Engineers, Part A: Journal of Power and Energy*. https://doi.org/10.1177/0957650912464922.

Baxter, Alexander, and Fredric Ehrich. 2024. "Jet Engine | Engineering, Design, & Functionality | Britannica." January 26, 2024. https://www.britannica.com/technology/jet-engine.

Bidkar, Rahul A, Edip Sevincer, Jifeng Wang, Azam M Thatte, Andrew Mann, Maxwell Peter, Grant Musgrove, Timothy Allison, and Jeffrey Moore. 2017. "Low-Leakage Shaft-End Seals for Utility-Scale Supercritical CO 2 Turboexpanders." https://doi.org/10.1115/1.4034258.

Bill, Robert C, and Lawrence P Ludwig. 1980. "WEAR OF SEAL MATERIALS USED IN AIRCRAFT PROPULSION SYSTEMS*." *Wear*. Vol. 59. Elsevier Sequoia S.A.

Bonolo De Campos, Gustavo, Cleverson Bringhenti, Alberto Traverso, and Jesuino Takachi Tomita. 2019. "A Review on Combining Micro Gas Turbines with Organic Rankine Cycles." *E3S Web of Conferences* 113 (August). https://doi.org/10.1051/E3SCONF/201911303007.

Boston, Amsterdam •, • Heidelberg, • London, New York, • Oxford, • Paris, • San, et al. 2014. "SIXTH EDITION SEALS AND SEALING HANDBOOK." http://elsevier.com/locate/permissions,.

Burcham, R. E. 1979. "NASA SPACE VEHICLE DESIGN CRITERIA (CHEMIC AL PROPUL SION) ROTA TING-SHAF T SEAL S FEBRUARY 1978 NATION AL AERON AUTICS AND SPACE ADMINI STRAT ION."

Bureau of Transportation Statistics. 2022. "U.S. Airlines' 2021 Total Fuel Use Decreases 25% from Pre-Pandemic 2019; December 2021 Fuel Use Down 13% from December 2019 | Bureau of Transportation Statistics." February 2, 2022. https://www.bts.gov/newsroom/us-airlines-2021-total-fuel-use-decreases-25-pre-pandemic-2019-december-2021-fuel-use-down.

Bureau of Transportation Statistics. 2023. "U.S. Airlines' January 2023 Fuel Cost per Gallon Up 4.3% from December 2022; Aviation Fuel Consumption Down 0.7% from Pre-Pandemic January 2019 | Bureau of Transportation Statistics." March 3, 2023. https://www.bts.gov/newsroom/us-airlines-january-2023-fuel-cost-gallon-43-december-2022-aviation-fuel-consumption-down.

Camatti, Massimo, and Giuseppe Vannini. 2003. “Instability of a High Pressure Compressor Equipped with Honeycomb Seals.” https://doi.org/10.21423/R1636F.

Campos, Gustavo Bonolo de, Cleverson Bringhenti, Alberto Traverso, Jesuino Takachi Tomita, Gustavo Bonolo de Campos, Cleverson Bringhenti, Alberto Traverso, and Jesuino Takachi Tomita. 2020. “Thermoeconomic Optimization of Organic Rankine Bottoming Cycles for Micro Gas Turbines.” *AppTE* 164 (January): 114477. https://doi.org/10.1016/J.APPLTHERMALENG.2019.114477.

Carcasci, Carlo, and Lorenzo Winchler. 2016. “Thermodynamic Analysis of an Organic Rankine Cycle for Waste Heat Recovery from an Aeroderivative Intercooled Gas Turbine.” *Energy Procedia* 101 (November): 862–69. https://doi.org/10.1016/J.EGYPRO.2016.11.109.

Cesmeci, Sevki, Ikenna Ejiogu, Md Mahmudur Rahman, Mohammad Fuad Hassan, Hanping Xu, and Jing Tang. 2023. “Numerical Modeling of an Elastohydrodynamic Seal Design for Supercritical CO2 Power Cycles.” *American Society of Mechanical Engineers, Power Division (Publication) POWER* 2023-August (September). https://doi.org/10.1115/POWER2023-108959.

Cesmeci, Sevki, Rubayet Hassan, Mohammad Fuad Hassan, Ikenna Ejiogu, Matthew DeMond, Hanping Xu, and Jing Tang. 2021. “An Innovative Elasto-Hydrodynamic Seal Concept for Supercritical CO2 Power Cycles.” *American Society of Mechanical Engineers, Power Division (Publication) POWER* 2021-July (August). https://doi.org/10.1115/POWER2021-64536.

Cesmeci, Sevki, Karthik Reddy Lyathakula, Mohammad Fuad Hassan, Shuangbiao Liu, Hanping Xu, and Jing Tang. 2022. “Analysis of an Elasto-Hydrodynamic Seal by Using the Reynolds Equation.” *Applied Sciences* 12 (19): 9501.

Chopra, Anil. 2019. “Emerging Trends in Aero Engine Technologies.” April 2019. https://www.spsairbuz.com/story/?id=941&h=Emerging-Trends-in-Aero-Engine-Technologies.

Chupp, Raymond E, Robert C Hendricks, Scott B Lattime, and Bruce M Steinetz. 2006a. “Sealing in Turbomachinery.” http://www.sti.nasa.gov.

Chupp, Raymond E., Robert C. Hendricks, Scott B. Lattime, and Bruce M. Steinetz. 2006b. “Sealing in Turbomachinery.” *Journal of Propulsion and Power* 22 (2): 313–49. https://doi.org/10.2514/1.17778.

Chupp, Raymond E., and Paul Nelson. 1993. “Evaluation of Brush Seals for Limited-Life Engines.” *Journal of Propulsion and Power* 9 (1): 113–18. https://doi.org/10.2514/3.11492.

Chupp, Raymond, Farshad Ghasripoor, and Gerald Moore. 2002. “APPLYING ABRADABLE SEALS TO INDUSTRIAL GAS TURBINES.”

Cich, Stefan D., Christina Twist, Inderpal Sihra, and Matt Taher. 2020. “Introduction to Dry Gas Seals and Systems.” https://oaktrust.library.tamu.edu/handle/1969.1/196844.

Dinc, Saim, Mehmet Demiroglu, Norman Turnquist, Jason Mortzheim, Gayle Goetze, John Maupin, James Hopkins, Christopher Wolfe, and Mark Florin. 2001. “Fundamental Design Issues of Brush Seals for Industrial Applications.” *Proceedings of the ASME Turbo Expo* 3: 1–10. https://doi.org/10.1115/2001-GT-0400.

Energy Information Administration, Us. 2024. “Monthly Energy Review – February 2024.” www.eia.gov/mer.

Feldermann, Achim, Stephan Neumann, and Georg Jacobs. 2017. “CFD Simulation of Elastohydrodynamic Lubrication Problems with Reduced Order Models for Fluid–Structure Interaction.” *Tribology - Materials, Surfaces and Interfaces* 11 (1): 30–38. https://doi.org/10.1080/17515831.2017.1279846.

Ferguson, J. G. 1988. “Brushes As High Performance Gas Turbine Seals.” *ASME 1988 International Gas Turbine and Aeroengine Congress and Exposition* 2 (ISBN: 978-0-7918-7919-1): 8. https://doi.org/10.1115/88-gt-182.

“GLOBAL FLEET & MRO MARKET FORECAST COMMENTARY.” 2018.

Gong, Ru Zhi, De You Li, Hong Jie Wang, Lei Han, and Da Qing Qin. 2016. “Analytical Solution of Reynolds Equation under Dynamic Conditions.” *Proceedings of the Institution of Mechanical Engineers, Part J: Journal of Engineering Tribology* 230 (4): 416–27. https://doi.org/10.1177/1350650115604654.

Grondahl, Clayton M., and James C. Dudley. 2010. “Film Riding Leaf Seals for Improved Shaft Sealing.” *Proceedings of the ASME Turbo Expo* 4 (PARTS A AND B): 1293–1300. https://doi.org/10.1115/GT2010-23629.

Hassan, Mohammad Fuad, Hanping Xu, Sevki Cesmeci, Md Wasif Hasan, Ali Akbor Topu, Mohammad Towhidul Islam, and Harcrow Aaron. 2024. “Experimental Investigation of an Elastohydrodynamic Seal for Supercritical CO2 Turbomachinery.” In *Proceedings of ASME Turbo Expo 2024*.

Hassan, Mohammad Fuad, Hanping Xu, Mohammad Towhidul Islam, and Cesmeci Sevki. 2024. “Experimental Demonstration of a Novel Supercritical Co 2 Seal Concept on a 2 ’’ Static Test Rig.” In *The 8th International Supercritical CO2 Power Cycles Symposium*, 1–22. San Antonio, Texas.

Hassan, Mohammad Fuad, Hanping Xu, Mohammad Towhidul Islam, Sevki Cesmeci, Shuangbiao Liu, Aaron Harcrow, Ali Akbor Topu, et al. 2024. “Experimental Demonstration of a Novel Elastohydrodynamic Seal Concept for SCO2 Turbomachinery,” February. https://doi.org/10.1115/IMECE2023-114172.

Heidmann, James D. 2013. “Improving Engine Efficiency Through Core Developments.” In . https://api.semanticscholar.org/CorpusID:106853723.

Henry, Jonah, Hanping Xu, Mohammad Fuad Hassan, Sevki Cesmeci, Mohammad Towhidul Islam, Shuangbiao Liu, and Jing Tang. 2023. “Experimental Analysis of an Elastohydrodynamic Seal for Supercritical Carbon Dioxide Turbomachinery.” *American Society of Mechanical Engineers, Power Division (Publication) POWER* 2023-August (September). https://doi.org/10.1115/POWER2023-108781.

Hühn, L., F. Rieger, F. Bleier, C. Schwitzke, H.-J. Bauer, and T. Behnisch. 2018. “Extensive Investigations on Radial Crack Formation in Labyrinth Seals of Aircraft Engines.” *Deutscher Luft- Und Raumfahrtkongress, Friedrichshafen, Deutschland, 4 - 6 September 2018*, 8. https://doi.org/10.25967/480120.

Hünecke, Klaus. 1997. “Jet Engines : Fundamentals of Theory, Design, and Operation.” *(No Title)*. https://cir.nii.ac.jp/crid/1130000797382743552.

Ibrahim, Amir, David Gillespie, and John Garratt. 2017. “Radial Pressure Distributions in an Air-Riding Face Seal.” https://hal.science/hal-02376826.

INTERNATIONAL CIVIL AVIATION ORGANIZATION. 2016. “On Board a Sustainable Future ENVIRONMENT.”

Islam, Mohammad Towhidul, Mohammad Fuad Hassan, Karthik Reddy Lyathakula, Sevki Cesmeci, Hanping Xu, and Jing Tang. 2023. “A Design Study of an Elasto-Hydrodynamic Seal for SCO2 Power Cycle by Using Physics Informed Neural Network.” *American Society of Mechanical Engineers, Power Division (Publication) POWER* 2023-August (September). https://doi.org/10.1115/POWER2023-108802.

Kemp, John. 2023. “U.S. Jet Fuel Shortage Drives Airline Costs Higher | Reuters.” February 16, 2023. https://www.reuters.com/markets/commodities/us-jet-fuel-shortage-drives-airline-costs-higher-kemp-2023-02-16/.

Khadse, Akshay, Lauren Blanchette, Jayanta Kapat, Subith Vasu, Jahed Hossain, and Adrien Donazzolo. 2018. “Optimization of Supercritical CO2 Brayton Cycle for Simple Cycle Gas Turbines Exhaust Heat Recovery Using Genetic Algorithm.” *Journal of Solar Energy Engineering, Transactions of the ASME* 140 (7). https://doi.org/10.1115/1.4039446/368563.

Kim, Min Seok, Seong Jun Bae, Seongmin Son, Bong Seong Oh, and Jeong Ik Lee. 2019. “Study of Critical Flow for Supercritical CO2 Seal.” *International Journal of Heat and Mass Transfer* 138: 85–95.

Li, Guoqing, Qian Zhang, Enliang Huang, Zhijun Lei, Hongwei Wu, and Gang Xu. 2019. “Leakage Performance of Floating Ring Seal in Cold/ Hot State for Aero-Engine.” https://doi.org/10.1016/j.cja.2019.03.004.

Li, Guoqing, Qian Zhang, Zhijun Lei, Enliang Huang, Hongwei Wu, and Gang Xu. 2019. “Leakage Performance of Labyrinth Seal for Oil Sealing of Aero-Engine.” *Propulsion and Power Research* 8 (1): 13–22. https://doi.org/10.1016/J.JPPR.2018.12.003.

LI, Guoqing, Shen ZHANG, Zhong KANG, Yanfeng ZHANG, Xingen LU, and Junqiang ZHU. 2022. “Leakage and Wear Characteristics of Carbon Seals for Aero-Engines.” *Chinese Journal of Aeronautics* 35 (11): 389–400. https://doi.org/10.1016/J.CJA.2021.11.002.

Liu, Rui. 2009. “Application of Tribology in Aircraft Engine Sealing Technology.”

Loomis, William R. 1984. “Tribology in the 80’s: Volume 2-Sessions 5 to 8.” National Aeronautics and Space Administration.

Ludwig, Ijay^ence P, and Lawrence P Ludwig. 1978. “Gas Path Sealing in Turbine Engines.”

Ludwig, L. P., and R. L. Johnson. 1974. “Sealing Technology for Aircraft Gas Turbine Engines.”

Ludwig, Lawrence P., and Robert C. Bill. 1980. “Gas Path Sealing in Turbine Engines.” *ASLE Transactions* 23 (1): 1–22. https://doi.org/10.1080/05698198008982942.

Lyathakula, Karthik Reddy, Sevki Cesmeci, Matthew DeMond, Mohammad Fuad Hassan, Hanping Xu, and Jing Tang. 2023. “Physics-Informed Deep Learning-Based Proof-of-Concept Study of a Novel Elastohydrodynamic Seal for Supercritical CO2 Turbomachinery.” *Journal of Energy Resources Technology* 145 (12). https://doi.org/10.1115/1.4063326.

Lyathakula, Karthik Reddy, Sevki Cesmeci, Matthew DeMond, Hanping Xu, and Jing Tang. 2022. “Physics-Informed Deep Learning-Based Modeling of a Novel Elastohydrodynamic Seal for Supercritical CO2 Turbomachinery.” *American Society of Mechanical Engineers, Power Division (Publication) POWER* 2022-July (September). https://doi.org/10.1115/POWER2022-86597.

Lyathakula, Karthik Reddy, Sevki Cesmeci, Mohammad Fuad Hassan, Hanping Xu, and Jing Tang. 2022a. “A Proof-of-Concept Study of a Novel Elasto-Hydrodynamic Seal for CO2.” In *ASME Power Conference*, 85826:V001T12A003. American Society of Mechanical Engineers.

———. 2022b. “A Proof-of-Concept Study of a Novel Elasto-Hydrodynamic Seal for CO2.” *American Society of Mechanical Engineers, Power Division (Publication) POWER* 2022-July (September). https://doi.org/10.1115/POWER2022-86607.

Lynwander, P. 1973. “Development of Helicopter Engine Seals.”

Macchi, Ennio, and Marco Astolfi. 2016. “Organic Rankine Cycle (ORC) Power Systems: Technologies and Applications.” September 2016. https://www.researchgate.net/publication/316937257_Organic_Rankine_Cycle_ORC_Power_Systems_Technologies_and_Applications.

Marchionni, Matteo, Giuseppe Bianchi, and Savvas A. Tassou. 2020. “Review of Supercritical Carbon Dioxide (SCO2) Technologies for High-Grade Waste Heat to Power Conversion.” *SN Applied Sciences* 2 (4): 1–13. https://doi.org/10.1007/S42452-020-2116-6/TABLES/5.

Millhouse, Paul T. 1998. “Improving Algorithmic Efficiency of Aircraft Engine Design for Optimal Mission Performance.” In . https://api.semanticscholar.org/CorpusID:107561666.

Moore, A. 1975. “Gas Turbine Engine Internal Air Systems: A Review of the Requirements and the Problems THE AMERICAN SOCIETY OF MECHANICAL ENGINEERS,-Asme/Terms-of-Use Gas Turbine Engine Internal Air Systems: A Review of the Requirements and the Problems.” http://www.asme.org/about-asme/terms-of-use.

Overton, Jeff. 2022. “Issue Brief | The Growth in Greenhouse Gas Emissions from Commercial Aviation (2019, Revised 2022) | White Papers | EESI.” June 9, 2022. https://www.eesi.org/papers/view/fact-sheet-the-growth-in-greenhouse-gas-emissions-from-commercial-aviation.

Pasini, S., I. Ghezzi, R. Andriani, and L.D.A. Ferri. 2002. “Heat Recovery from Aircraft Engines,” November, 546–53. https://doi.org/10.1109/IECEC.2000.870782.

Plehwe, Felix C von, Matthias B Krug, and org Bauer. 2016. “EXPERIMENTAL AND NUMERICAL INVESTIGATIONS ON OIL LEAKAGE ACROSS LABYRINTH SEALS IN AERO ENGINE BEARING CHAMBERS.”

http://proceedings.asmedigitalcollection.asme.org/pdfaccess.ashx?url=/data/conferences/asmep/89467/.

Pröstler, Stephan. 2002. “CFD Modeling of Brush Seals.” In *European CFX Conference*, 16:18.

Ritchie, Hannah. 2020. “Climate Change and Flying: What Share of Global CO2 Emissions Come from Aviation? - Our World in Data.” October 22, 2020. https://ourworldindata.org/co2-emissions-from-aviation#article-citation.

Rossmann, Axel. 2023. “23.4.1 Static Seals, O-Ring Seals [Aeroengine Safety].” January 12, 2023. https://aeroenginesafety.tugraz.at/doku.php?id=23:234:2341:2341.

Schriber, Johannes. 2016. “Investigation of Experimental and Numerical Methods,and Analysis of Stator Clockingand Instabilitiesinahigh-Speedmultistage Compre,” December. https://doi.org/10.13140/RG.2.2.31489.86881.

Sens, William H. 1979. “AIRCRAFT ENGINE DEVELOPMENTS CENTRE ON IMPROVED PERFORMANCE, HIGHER EFFICIENCY.” *ICAO BULLETIN* 34. https://api.semanticscholar.org/CorpusID:107063916.

Shabbir, Sarah, Seamus Garvey, and Sam M Dakka. 2019. “Aerospace Sealing Technology for Maintenance, Repair and Overhaul of Engines: A Review.”

Shaw, Robert. 2021. “Engines.” May 13, 2021. https://www.grc.nasa.gov/www/k-12/UEET/StudentSite/engines.html.

Stakenborg, M. J.L. 1988. “On the Sealing Mechanism of Radial Lip Seals.” *Tribology International* 21 (6): 335–40. https://doi.org/10.1016/0301-679X(88)90110-7.

“Steam Turbines and Turboexpanders.” 1997. *Practical Machinery Management for Process Plants* 4 (C): 329–441. https://doi.org/10.1016/S1874-6942(97)80010-7.

Steinetz, B., R. Hendricks, and J. Munson. 1999. “Advanced Seal Technology Role in Meeting Next Generation Turbine Engine Goals.”

Steinetz, Bruce M, Robert C Hendricks, and John Munson. 1998. “Advanced Seal Technology Role in Meeting Next Generation.” *Design Principles and Methods for Aircraft Gas Turbine Engines*, no. May: 11–15. http://hdl.handle.net/2060/19980201334.

Vesely, Ladislav, Cleverson Bringhenti, Jesuino Takachi Tomita, and Michael Stoia. 2022. “SCO2 Waste Heat Recovery System in Aircraft Engine.” https://doi.org/10.2514/6.2022-1407.

Vesely, Ladislav, Prabu Thangavel, S Gopinathan, Otakar Frybort, Ganesan Subbaraman, and Jayanta Kapat. 2021. “GREENING A CEMENT PLANT USING SCO 2 POWER CYCLE The 4 Th European SCO 2 Conference for Energy Systems March 22-26, 2021, Prague, Czech Republic.”

Wong, P. L., H. Xu, and Z. Zhang. 1997. “Performance Evaluation of High Pressure Sleeve Seal.” *Wear* 210 (1–2): 104–11. https://doi.org/10.1016/S0043-1648(97)00050-1.

Wu, Tingcheng, and Luis San Andrés. 2019. “Gas Labyrinth Seals: On the Effect of Clearance and Operating Conditions on Wall Friction Factors – A CFD Investigation.” *Tribology International* 131 (October 2018): 363–76. https://doi.org/10.1016/j.triboint.2018.10.046.

Xu, H. P., P. L. Wong, and Z. M. Zhang. 1999. “An EHL Analysis of an All-Metal Viscoelastic High-Pressure Seal.” *Journal of Tribology* 121 (4): 916–20. https://doi.org/10.1115/1.2834155.

Xu, Hanping, and Tianjue Lei. 1994. “A Ringless High Pressure Moving Seal up to 1200 Mpa.” *Tribology Transactions* 37 (4): 767–70. https://doi.org/10.1080/10402009408983358.

Zhao, Hailin, Hua Su, and Guoding Chen. 2020. “Analysis of Total Leakage of Finger Seal with Side Leakage Flow.” *Tribology International* 150: 106371. https://doi.org/10.1016/j.triboint.2020.106371.